

DNDI-6148: A Novel Benzoxaborole Preclinical Candidate for the Treatment of Visceral Leishmaniasis

Charles E. Mowbray,* Stéphanie Braillard, Paul A. Glossop, Gavin A. Whitlock, Robert T. Jacobs, Jason Speake, Bharathi Pandi, Bakela Nare, Louis Maes, Vanessa Yardley, Yvonne Freund, Richard J. Wall, Sandra Carvalho, Davide Bello, Magali Van den Kerkhof, Guy Caljon, Ian H. Gilbert, Victoriano Corpas-Lopez, Iva Lukac, Stephen Patterson, Fabio Zuccotto, and Susan Wyllie*



Cite This: *J. Med. Chem.* 2021, 64, 16159–16176



Read Online

ACCESS |



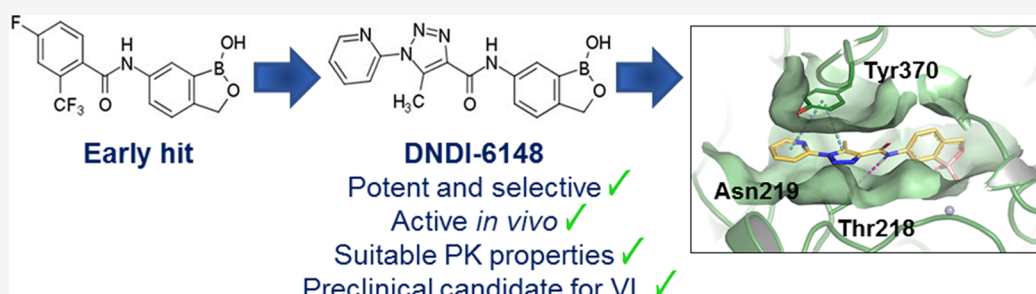
Metrics & More



Article Recommendations



Supporting Information



ABSTRACT: Visceral leishmaniasis (VL) is a parasitic disease endemic across multiple regions of the world and is fatal if untreated. Current therapies are unsuitable, and there is an urgent need for safe, short-course, and low-cost oral treatments to combat this neglected disease. The benzoxaborole chemotype has previously delivered clinical candidates for the treatment of other parasitic diseases. Here, we describe the development and optimization of this series, leading to the identification of compounds with potent *in vitro* and *in vivo* antileishmanial activity. The lead compound (DNDI-6148) combines impressive *in vivo* efficacy (>98% reduction in parasite burden) with pharmaceutical properties suitable for onward development and an acceptable safety profile. Detailed mode of action studies confirm that DNDI-6148 acts principally through the inhibition of *Leishmania* cleavage and polyadenylation specificity factor (CPSF3) endonuclease. As a result of these studies and its promising profile, DNDI-6148 has been declared a preclinical candidate for the treatment of VL.

INTRODUCTION

Visceral leishmaniasis (VL) is a poverty-linked disease,¹ and occurs primarily in poor populations across Asia, East Africa, and South America.² Current estimates suggest 50 000–90 000 new cases of VL occur each year.³ VL is caused by infection with the protozoan parasites *Leishmania donovani* and *Leishmania infantum*, with transmission mediated by the bite of the female phlebotomine sand fly. Once the human host is infected, parasites survive and multiply within macrophages, leading to symptoms including prolonged fever, enlarged spleen and liver, substantial weight loss, and progressive anemia.⁴ If left untreated, the vast majority of clinically symptomatic VL patients die within months.

The current standard treatment for patients with VL in East Africa is sodium stibogluconate (SSG) combined with paromomycin (PM).⁴ In South-East Asia, the standard treatment is liposomal amphotericin B (LAB), with paromomycin and miltefosine as a second-line treatment option.⁵ While these combination approaches are more effective than SSG monotherapy, the mainstay of VL treatment for many

years, they still have significant limitations such as cost, route of administration (all given via the parenteral route apart from the oral drug miltefosine), and toxicity. Consequently, there is an ongoing need for effective new treatments that are easy to administer via oral dosing, are effective against VL in different regions of the world, have an improved safety profile, and are affordable for the patients who require them. Research and development for the treatment of VL has evolved rapidly in recent years, with 5 drug candidates from 4 different classes now in phase-1 clinical studies (Table 1).⁶

Here, we outline the optimization of a benzoxaborole series toward a possible new therapy for VL. The benzoxaborole class of compounds has already successfully delivered a clinical

Received: August 19, 2021

Published: October 29, 2021



Table 1. Current Portfolio of VL Drug Candidates in Clinical Development^a

compound ID	compound class	mechanism of action and/or molecular target	organization
DNDI-6148 ⁶	benzoxaborole	CPSF3	DNDi/Pfizer
DNDI-0690 ⁶	nitroimidazole	bioactivation by NTR2 ⁷	DNDi/TB Alliance
GSK3186899/DDD853651 ^{6,7}	pyrazolopyrimidine	CRK12 (cyclin-dependent kinase) ⁸	GSK/DDU
GSK3494245/DDD1305143 ^{6,8}	imidazopyridine	proteasome inhibitor ⁹	GSK/DDU
LXE408 ⁹	triazolopyrimidine	proteasome inhibitor ¹⁰	Novartis

^aDDU: Drug Discovery Unit, University of Dundee and GSK: GlaxoSmithKline.

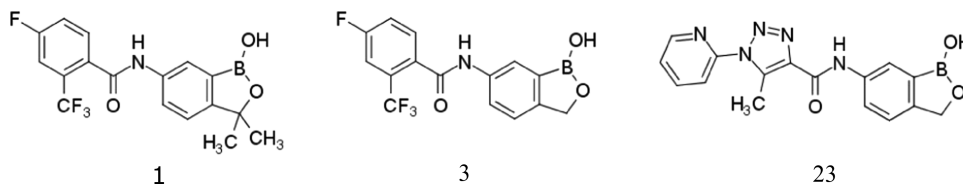


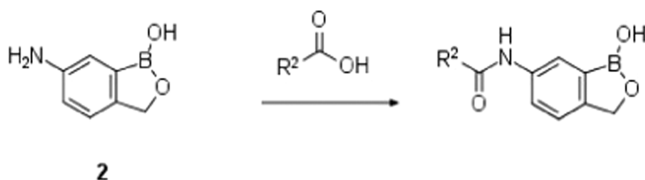
Figure 1. Structures of acoziborole (1), early hit 3, and preclinical candidate DNDI-6148 (23).

candidate (acoziborole, AN5568, **1**, Figure 1) for the treatment of stage 1 and stage 2 human African trypanosomiasis (HAT, African sleeping sickness).¹¹ Stimulated by the success of the acoziborole program, modifications to the benzoxaborole template were undertaken to identify novel compounds that may have utility for the treatment of VL, leading to the discovery of a preclinical candidate **23** (DNDI-6148). This compound combines good *in vitro* potency against both *L. infantum* and *L. donovani* alongside very high levels of *in vivo* efficacy (>98% reduction in parasite burden) in hamster models of infection. In addition, DNDI-6148 possesses excellent pharmacokinetics and is predicted to have acceptable human pharmacokinetics and an efficacious dose consistent with the requirements of the published target candidate (TCP) and target product (TPP) profiles for VL published by DNDi. Clinical trials with DNDI-6148 are now underway.¹¹

RESULTS AND DISCUSSION

Chemistry. The synthesis of benzoxaborole target compounds **3–31** consisted of amide bond formation between the key intermediate **2** and an appropriately functionalized acid (Scheme 1) using one of three coupling methods, whose

Scheme 1. General Synthesis of Amides **4–31**^a



^aReagents and conditions: Method A: HOBt, EDCI, *N,N*-diisopropylethylamine (DIPEA), CH₂Cl₂, rt, 2 h, 66%; Method B: HATU, DIPEA, *N,N*-dimethylformamide (DMF), rt, 16 h, 8–77%; and Method C: (i) SOCl₂, 50 °C, 4 h, (ii) DIPEA, tetrahydrofuran (THF), rt, 16 h, 4–68%.

choice was driven by substrate compatibility: Method A (HOBt/EDCI coupling), Method B (HATU coupling), and Method C (acid chloride formation using SOCl₂ followed by coupling with intermediate **2**). The synthesis of the carboxylic acid intermediates R²CO₂H is described in detail in the Supplementary Information. Example **12** was synthesized using Method A. Examples **4**, **6–11**, **13–15**, **17–18**, **20–21**, **23–27**,

and **29–30** were synthesized using Method B, while examples **5**, **16**, **19**, **22**, **28**, and **31** were synthesized using Method C.

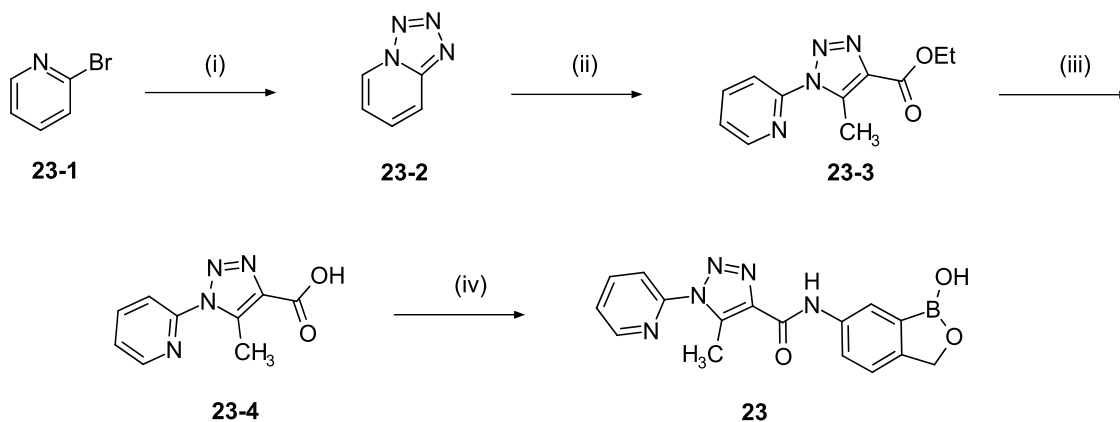
Preclinical candidate compound **23** was synthesized using a 4-step synthesis (Scheme 2).

Formation of the fused tetrazole **23-2** was achieved by the reaction of 2-bromopyridine with sodium azide. Cyclo-addition of **23-2** with ethyl 3-oxobutanoate gave the N1-substituted triazole **23-3**, which was hydrolyzed to the corresponding acid **23-4**. Coupling benzoxaborole scaffold **2** using Method B gave the final compound **23** in high overall yield.

Compound **1** was potent in *in vitro* assays against *Trypanosoma brucei*, the etiological agent of HAT (EC₅₀ value of 795 nM),¹² but demonstrated only weak activity in intramacrophage assays with both *L. infantum* and *L. donovani* (Table 2). It should be noted that *L. infantum*-derived infections can be refractory to some current drug therapies. Thus, new compounds in development are screened against both *L. infantum* and *L. donovani* at an early stage to ensure efficacy. However, the close analogue **3** (SCYX-6759), lacking the gem-dimethyl substitution on the benzoxaborole ring, was considerably more potent in these assays.¹³

Previous studies demonstrated that compound **3** has low clearance in multiple animal models and is efficacious in a murine model of HAT.¹³ Consequently, compound **3** was progressed to an *L. infantum* hamster model of VL infection (Table 3).¹⁴ Compound **3** was highly efficacious at QD doses of 50 and 100 mg/kg, virtually clearing all parasites from the liver and spleen. However, reductions in parasite burden in the bone marrow were more modest and thus failed to meet the DNDi target candidate profile (TCP) of >95% reduction in parasite burden. Therefore, additional benzoxaboroles were synthesized to identify compounds that were highly efficacious in all tissues across a broad dose range.

The simplified benzoxaborole ring system, with the gem-dimethyl substitution on the benzoxaborole ring removed, was retained in subsequent analogues and the amide substituent became the focus for development. Replacing the lipophilic aryl substituent with a more polar heteroaryl group was investigated in detail to reduce the lipophilicity to values more associated with orally bioavailable drugs.¹⁵ Consistent with this design strategy, a range of substituted pyrazoles was synthesized (Table 4). Excellent levels of *in vitro* potency were achieved with compounds **4–6**, which contain a trifluoromethyl R¹ substituent and a fluorinated *N*-alkyl R²

Scheme 2. Synthesis of Compound 23^a

^aReagents and conditions: (i) NaN_3 , CuI , NaOAc , DMEDA , EtOH , H_2O , 1 h, reflux, 94%; (ii) ethyl 3-oxobutanoate, NaOEt , EtOH , 48 h, reflux; (iii) NaOH , H_2O , EtOH , 20 h, 45 °C, 48% for (ii) and (iii); and (iv) **2**, HATU, DIPEA, DMF, room temperature (RT), 3 h, 74%. Note, the material subsequently used in the mode of action studies was prepared from commercially available **23-2** via a modification of this route (see Scheme 5).

Table 2. Collated EC_{50} Values for Compounds 1, 3 and the Current Front-Line Antileishmanial Miltefosine

compound	EC_{50} values, μM^a		PMM
	intramacrophage <i>L. donovani</i>	intramacrophage <i>L. infantum</i>	
1	59	>64	>64
3	1.2	2.7	>64
23	1.4	1.8	>64
miltefosine	10	10	33

^aGeometric mean value of at least three independent assays. PMM: primary mouse macrophages.

Table 3. *In Vivo* Efficacy of Compound 3 in an *L. infantum* Hamster Model of VL, after QD Dosing for 5 Days^a

dose (mg/kg)	reduction in parasite burden, %		
	liver	spleen	bone marrow
25	87.8	81.8	81.6
50	97.4	95.0	91.2
100	98.6	96.0	88.3

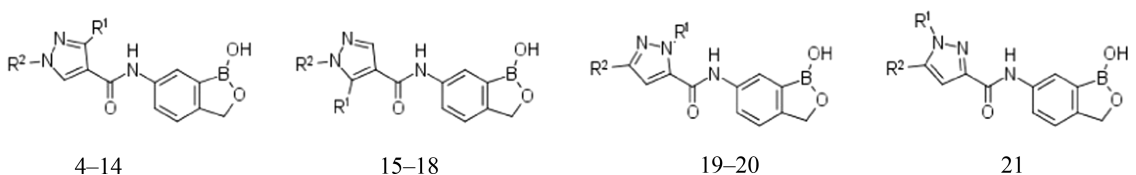
^a $n = 6$ animals per group, results were expressed as a percentage reduction in amastigote burden compared to vehicle-treated, infected control animals.

substituent. Importantly, compounds **4–6** showed no evidence of cytotoxicity ($\text{CC}_{50} > 38 \mu\text{M}$) in the counter-screen with PMM. These analogues also had excellent *in vitro* metabolic stability in HLM, but compounds **4** and **6** had poor stability in hamster liver microsomes (HamLM), which precluded their evaluation in the *in vivo* hamster model of VL. Compound **5** combined sufficient *in vitro* potency, selectivity index (SI), and stability in both HLM and HamLM to be considered for further progression. Compound **7** ($\text{R}^1 = \text{Me}$) was slightly less potent than its CF_3 analogue **6**, and this same trend was also observed for the *N*-cyclobutyl examples **8** and **9** as well as for the 2-pyridyl examples **11** and **12**. However, the CF_3 -substituted analogues **6**, **9**, and **12** were all more cytotoxic in PMM than their CH_3 -substituted counterparts **7**, **8**, and **11**. Tetrahydropyran-yl-substituted analogue **10** combined many of the necessary properties, but HamLM stability was insufficient to deliver enough *in vivo* exposure for efficacy studies.

Typically, a HamLM clearance of $<100 \mu\text{L}/\text{min}/\text{mg}$ is required to observe meaningful exposure *in vivo*. Further lipophilic aryl R^2 substituents such as 4-Cl-phenyl **13** and 2-MeO-phenyl **14** had potent *in vitro* *L. infantum* activity but were cytotoxic in PMM and/or MRC5 cells. The pyrazole **15** exhibited a significant drop in potency compared to its isomeric analogue **6**, whereas the pyridyl-substituted compound **16** was slightly more potent than its isomer **11**. Further substituted pyridine examples **17** and **18** were also potent and demonstrated good SI. In addition, compounds **16–18** were stable in both HLM and HamLM. Additional pyrazole isomers **19–21** all failed to combine sufficient *in vitro* potency and weak cytotoxicity with good metabolic stability.

Of the compounds made up to this point, 2-pyridyl-substituted analogue **16** was one of the most interesting as it combined good *in vitro* potency, low lipophilicity, promising SI, and was stable in both HLM and HamLM. For the next set of compounds, the 2-pyridyl substituent was retained and further changes to the 5-membered heterocycle were investigated (Table 5). Triazole **22**, where $\text{R}^1 = \text{H}$, showed an encouraging improvement in both *in vitro* potency and HamLM stability over pyrazole **16**. The Me-substituted example **23** had an even better profile with high levels of *L. infantum* potency, no sign of cytotoxicity in PMM and MRC5, and very high levels of metabolic stability in HLM and HamLM. Further 1,2,3-triazoles demonstrated that the 2-pyridyl substituent was important; for example, the phenyl example **24** and 3-pyridyl example **27** had significantly weaker *in vitro* potency. Substitution on the 2-pyridyl group could be tolerated, with the 6-OMe analogue **25** showing an improved potency profile but at the expense of metabolic stability. The 6-Me compound **26** lost some potency and was therefore not progressed to metabolic stability assessment. Furan example **28** was very potent, and although it did exhibit some cytotoxicity in both PMM and MRC5, the high level of potency meant that **28** still retained a high SI. Despite being more lipophilic, metabolic stability was retained in both HLM and HamLM and, therefore, **28** was considered for further progression. The isomeric furan **29** had slightly reduced potency and SI compared to **28**, and the thiophene **30** was highly cytotoxic in MRC5 cells. The more polar oxadiazole **31** delivered a good overall profile and was also considered for further progression.

Table 4. Antileishmanial Activity of Pyrazoles 4–21

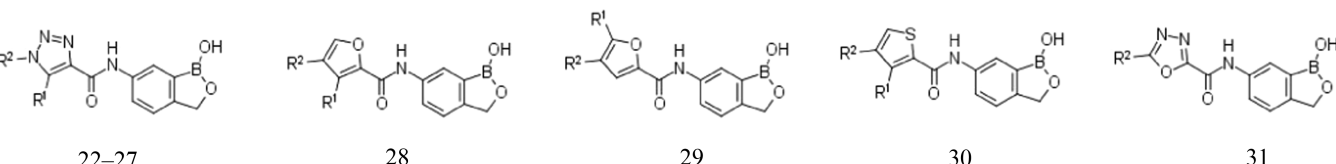


Chemical structures of pyrazoles 4–21 are shown above the table. They consist of a pyrazole ring substituted with R¹ and R² groups, connected via a carbonyl group to a benzimidazole moiety.

compound	R ¹	R ²	intramacrophage <i>L. infantum</i> EC ₅₀ (μM) ^a	PMM ^a CC ₅₀ (μM)	MRC5 ^a		HLM	HamLM
					CC ₅₀ (μM)	SI ^b	Cl _{int} (μL/min/mg)	
3			2.7	>64	>64	>24	0.8	n.d.
4	CF ₃	CF ₃	2.1	>64	>64	>31	<11.9	1,035
5	CF ₃	CH ₂ CF ₃	1.6	50	>64	>40	<11.9	41
6	CF ₃	(CH ₂) ₂ CF ₃	1.3	38	49	38	<11.9	114
7	CH ₃	(CH ₂) ₂ CF ₃	5.7	>64	>64	>11	n.d.	n.d.
8	CH ₃	c-butyl	16	>64	>64	>4	<11.9	57
9	CF ₃	c-butyl	0.59	32	26	53	<11.9	337
10	CF ₃	4-THP	3.0	>64	>64	>21	<11.9	109
11	CH ₃	2-pyridyl	5.7	>64	>64	>11	<11.9	n.d.
12	CF ₃	2-pyridyl	0.64	2.0	1.1	1.6	n.d.	n.d.
13	CF ₃	4-Cl-phenyl	1.3	8.0	2.6	2	n.d.	n.d.
14	CH ₃	2-MeO-phenyl	2.2	>64	15.7	7.3	n.d.	n.d.
15	CH ₃	(CH ₂) ₂ CF ₃	14	>64	>64	>5	<11.9	48
16	CH ₃	2-pyridyl	3.1	59	61	15	<11.9	57
17	CH ₃	2-pyridyl-6-OMe	1.4	>64	40	31	<11.9	40
18	CH ₃	2-pyridyl-6-Me	1.6	>64	41	25	<11.9	44
19	H	2-pyridyl	0.5	32	4.0	8	<11.9	253
20	CH ₃	2-pyridyl	34	>64	>64	>2	18	121
21	CH ₃	2-pyridyl	1.8	>64	54	31	14	106
miltefosine			10	33	>64	>6.2	n.d.	n.d.

^aGeometric mean value of at least two independent tests. ^bSelectivity index representing the ratio of CC₅₀/EC₅₀; data are presented as the geometric mean value of ratios calculated using separate data from at least two independent tests. n.d., not determined.

Table 5. Antileishmanial Activity of Compounds 22–31



Chemical structures of compounds 22–31 are shown above the table. They consist of a pyrazole ring substituted with R¹ and R² groups, connected via a carbonyl group to a benzimidazole moiety.

compound	R ¹	R ²	intramacrophage <i>L. infantum</i> amastigote EC ₅₀ (μM) ^a	PMM ^a CC ₅₀ (μM)	MRC5 ^a		HLM	HamLM
					CC ₅₀ (μM)	SI ^b	Cl _{int} (μL/min/mg)	
22	H	2-pyridyl	1.7	>64	44.8	30	<11.9	18
23	CH ₃	2-pyridyl	1.8	>64	>64	>39	<11.9	<11.9
24	CH ₃	phenyl	37	>64	>64	>1.7	<11.9	n.d.
25	CH ₃	2-pyridyl-6-OMe	0.8	32	>64	>80	23	40
26	CH ₃	2-pyridyl-6-Me	6.4	>64	>64	>10	n.d.	n.d.
27	CH ₃	3-pyridyl	38	>64	>64	>1.8	n.d.	n.d.
28	CH ₃	2-pyridyl	0.5	49	18	37	<11.9	40
29	CH ₃	2-pyridyl	1.7	29	45	18	<11.9	82
30	CH ₃	2-pyridyl	0.6	32	2.3	4	<11.9	88
31		2-pyridyl	2.0	>64	>64	>32	19	12

^aGeometric mean value of at least two independent tests. ^bSelectivity index representing the ratio of CC₅₀/EC₅₀; data are presented as the geometric mean value of ratios calculated using separate data from at least two independent tests. n.d., not determined.

The most promising compounds from this SAR investigation, namely 5, 16, 23, 28, and 31, were also assessed for their *in vitro* macrophage potency using intracellular *L. donovani* (Table 6). Pleasingly, four of these compounds retained excellent levels of *L. donovani* potency; however, the

oxadiazole 31 was about 5-fold weaker against *L. donovani* compared with its *L. infantum* potency.

Compounds 5, 16, 23, 28, and 31 were also progressed to hamster oral pharmacokinetic (PK) studies and an *L. infantum* model of VL in hamsters (Table 7). Triazole 23 exhibited noticeably higher exposure after a single oral dose of 50 mg/kg

Table 6. Antileishmanial Activity of Selected Compounds against *L. donovani*

compound	intramacrophage <i>L. infantum</i> EC ₅₀ (μM) ^a	intramacrophage <i>L. donovani</i> EC ₅₀ (μM) ^a	PMM ^a CC ₅₀ (μM)	MRC5 ^a	
				CC ₅₀ (μM)	SI ^b
5	1.6	1.0	53.8	>64	>64
16	3.1	1.2	>64	61.1	52
23	1.8	1.4	>64	>64	>46
28	0.5	0.4	54	18	45
31	2.0	9.4	>64	>64	>7

^aGeometric mean value of at least two independent tests. ^bSelectivity index representing the ratio of CC₅₀/EC₅₀; data are presented as the geometric mean value of ratios calculated using separate data from at least two independent tests.

Table 7. Oral Exposure and *In Vivo* Efficacy of Selected Compounds in an *L. infantum* Hamster Model of VL Following BID Dosing for 5 and 10 Days^a

compound	dose (mg/kg), BID	reduction in parasite burden, %						AUC _{0–24} after single p.o. dose of 50 mg/kg (h.ng/mL)
		liver		spleen		bone marrow		
		5 days	10 days	5 days	10 days	5 days	10 days	
5	25	89.7	n.d.	90.0	n.d.	77.0	n.d.	21 000
	50	99.7	n.d.	99.2	n.d.	98.0	n.d.	
16	25	87.8	n.d.	87.7	n.d.	72.2	n.d.	7900*
	50	99.6	n.d.	98.5	n.d.	95.1	n.d.	
23	25	98.3	100	98.2	99.9	93.6	99.4	120 000
	50	99.8	n.d.	99.9	n.d.	99.0	n.d.	
28	25	98.9	99.4	97.8	96.9	95.7	84	21 000
	50	99.9	n.d.	99.9	n.d.	99.1	n.d.	
31	25	67.3	n.d.	69.0	n.d.	55.0	n.d.	21 000
	50	99.4	n.d.	99.4	n.d.	99.7	n.d.	

^a*n* = 6 animals per group, the results are expressed as a percentage reduction in amastigote burden compared to vehicle-treated, infected control animals, *Study run using a single 25 mg/kg p.o. dose.

Table 8. *In Vivo* Efficacy of Selected Compounds in an *L. donovani* Hamster Model of VL Following BID Dosing for 5 and 10 Days^a

compound	dose (mg/kg), BID	reduction in parasite burden, %					
		liver		spleen		bone marrow	
		5 days	10 days	5 days	10 days	5 days	10 days
23	25	n.d.	99.9	n.d.	99.8	n.d.	99.6
	50	99.3	n.d.	98.6	n.d.	83.4	n.d.
28	25	95.9	n.d.	95.9	n.d.	94.5	n.d.
	50	99.9	n.d.	100	n.d.	100	n.d.

^a*n* = 6 animals per group, results were expressed as a percentage reduction in amastigote burden compared to vehicle-treated, infected control animals, n.d., not determined.

compared with the other lead compounds, which is consistent with its higher *in vitro* stability in HamLM and indicated that *in vitro* metabolic clearance may be predictive of *in vivo* clearance for this set of compounds.

All five compounds demonstrated excellent efficacy, with parasitemia significantly reduced in all organs after a dose of 50 mg/kg BID for 5 days. Triazole **23** and furan **28** also maintained excellent efficacy at a lower dosing of 25 mg/kg BID, consistent with the combination of good potency and high exposure observed for **23** and the very high potency of **28**. Extending the duration of treatment from 5 to 10 days for compound **23** led to almost complete eradication of parasites in the liver, spleen, and bone marrow. In contrast, the efficacy profile of compound **28** was not improved by extending the dosing period.

Compounds **23** and **28** were then studied in an *L. donovani* hamster model (Table 8). Triazole **23** exhibited high levels of efficacy in the liver and spleen when dosed orally at 50 mg/kg

BID for 5 days, although the reduction in parasite load in bone marrow was lower than the target of 95%. However, by extending the dosing period to 10 days, very high efficacy across all three tissues was achieved at a dose of 25 mg/kg BID. In addition, furan **28** achieved excellent efficacy in all tissues at both 25 mg/kg BID and 50 mg/kg BID for 5 days. These important data demonstrated that for both *L. infantum* and *L. donovani*, potent *in vitro* and *in vivo* activity could be achieved.

Compounds **23** and **28** were also assessed in mouse models of *L. donovani* and *L. infantum*; data confirmed that the high levels of efficacy observed in the chronic hamster model of infection was also achieved in the acute mouse model (Table 9).

Based on their *in vitro* potency, metabolic stability, and *in vivo* pharmacokinetic and efficacy profiles, compounds **23** and **28** were investigated in more detail to determine if either could be progressed to further preclinical development. Encouraged

Table 9. *In Vivo* Efficacy of Selected Compounds in *L. donovani* and *L. infantum* Mouse Models of VL Following BID Dosing for 5 Days

compound	dose (mg/kg), BID	reduction in liver parasite burden following 5 days of p.o. dosing BID ^a , %	
		<i>L. infantum</i>	<i>L. donovani</i>
23	25	96.1	97.1
	50	98.6	99.7
28	25	n.d.	97.5
	50	n.d.	99.5

^a*n* = 5 animals per group, the results were expressed as a percentage reduction in parasite burden compared to vehicle-treated, infected control animals, n.d., not determined.

by the outstanding *in vivo* efficacy of compound **28**, a 14-day exploratory toxicology study was conducted in male and female Sprague-Dawley rats. Unfortunately, compound **28** caused significant multiorgan toxicity following daily dosing of 25 mg/kg and the NOAEL (No Observed Adverse Effect Level) was not determined (<12.5 mg/kg). Consequently, further development of compound **28** was halted.

One potential concern associated with compound **28** was the presence of the furan, a functional group that can undergo oxidative metabolism to reactive metabolites.¹⁶ Thus, **23** and **28** were investigated to determine potential routes of metabolism and to understand if protein–ligand adducts were formed when the compounds were incubated in microsomes in the presence of glutathione. Metabolite identification studies with compound **28** showed evidence of ring-opening of the furan to an enone M-12 metabolite in all species tested (rat, mouse, dog, human, hamster). This metabolite has the potential to undergo conjugation to form protein–ligand adducts (Scheme 3).

In contrast, incubation of triazole **23** with microsomes indicated very limited metabolism, with only small amounts of mono-oxidation and hydrolysis/oxidative deboronation observed in dog and human microsomes, respectively (Scheme 4). No metabolism was detected in rat microsomes, and no evidence of reactive metabolite formation was found in any species.

In addition to the safety signals raised by a moderate *in vitro* activity against the MRC5 cell line (Table 5) and the lack of efficacy improvement when treatment duration was extended in the hamster model (Table 7), these *in vitro* metabolic studies clearly identified a potential weakness with furan **28** that may contribute to the observed *in vivo* toxicity. Therefore, **23** was prioritized for further evaluation. CYP inhibition was weak (IC₅₀ > 50 μM vs CYP1A2, 2C9, 2C19, 3A4, 2D6), hERG selectivity was high (hERG inhibition < 20% at 30 μM), and no activity > 50% was observed when **23** was tested in a panel of 88 targets (Cerep panel, Figure S13) at a concentration of 10 μM. Plasma-protein binding was moderate and consistent across species (dog 87%, human 92%, mouse 93%, rat 92%, hamster 88%). Thermodynamic solubility in

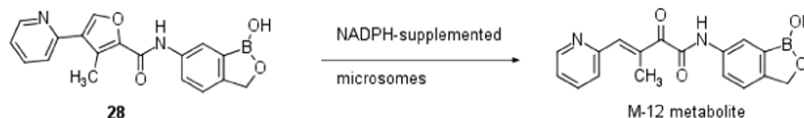
physiologically relevant media was low to moderate (Fasted State Simulated Intestinal Fluid, FaSSIF solubility = 5.4 μg/mL, Fed State Simulated Intestinal Fluid, FeSSIF solubility = 6.3 μg/mL), and membrane permeability was good with no evidence of P-gp-mediated efflux (MCDK efflux ratio of 0.7, Table S3). Microsome and hepatocyte stability was excellent across all species (Table 10), although hepatocyte stability was slightly worse in dogs compared with rats, monkeys, and humans. Compound **23** was also negative when tested in an Ames assay (TA98 and TA100 bacterial strains) with and without metabolic activation over a dose range from 1.5 to 1000 μg/well, suggesting no clastogenicity. To complete the early safety profile of compound **23**, a 14-day exploratory toxicology study was conducted in male and female Sprague-Dawley rats where the no adverse effect limit was set at 50 mg/kg/day.

In vivo pharmacokinetics after i.v. and p.o. dosing was determined in rats and dogs (Table 11 and Figure S12). Clearance in rats was low (4.5 mL/min/kg) with comparatively higher clearance in dogs (13.7 mL/min/kg), in line with the higher turnover in dog hepatocytes compared with rat hepatocytes. Oral bioavailability in rats was very high, indicating complete oral absorption. Bioavailability was somewhat lower in dogs and not fully understood at this point, but still acceptable for future progression of the compound. Allometric scaling from available rat and dog PK data suggests that compound **23** will have low clearance (Cl = 1–4 mL/min/kg) and moderate–high bioavailability (40–90%) in humans. BID dosing in humans at 3–20 mg/kg is predicted to achieve the efficacious exposure observed in the *L. infantum* and *L. donovani* hamster and mouse models of VL.

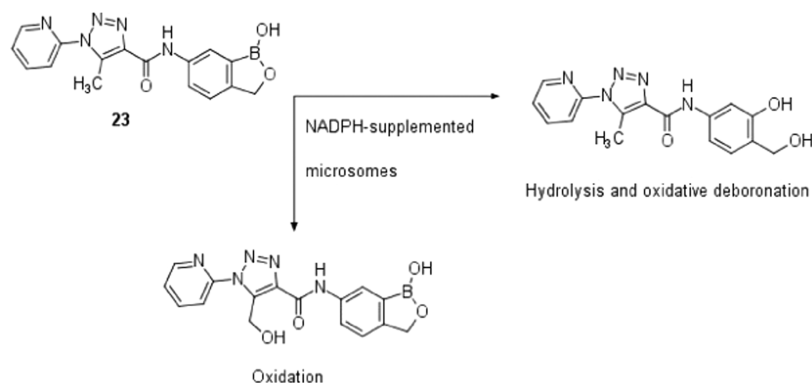
Mode of Action Studies (MoA). MoA studies as an integrated part of a drug discovery program can provide vital information that can be used to combat the high failure rates associated with the development of phenotypically active compounds. The association of active compounds with defined molecular targets during the development process can be extremely powerful. Understanding compound MoA can allow toxic liabilities associated with the target to be directly assessed, prevent enrichment of drug candidates against the same molecular target, and halt the development of inhibitors with an unattractive or invalidated target. Furthermore, this knowledge can inform future drug combination strategies.

Our previous studies with acoziborole (AN5568, **1**), in clinical development for HAT, revealed that this promising benzoxaborole specifically targets the Cleavage and Polyadenylation Specificity Factor 3 (CPSF3) in *T. brucei*.^{17–19} Additional compounds from within this series were also shown to target CPSF3, including **3**.^{13,19} CPSF3 is an endonuclease that forms part of the CPSF complex, involved in the control of polyadenylation and trans-splicing of pre-mRNA. Indeed, CPSF3 orthologues have also been identified as the molecular targets of benzoxaboroles active against *Plasmodium falciparum*,²⁰ *Toxoplasma gondii*,²¹ and *Cryptosporidium* spp.²¹ With this in mind, we hypothesized that DNDI-6148 (**23**) might

Scheme 3. Metabolic Fate of Compound **28** in the Presence of Microsomes from Multiple Species



Scheme 4. Metabolic Fate of Compound 23 in the Presence of Microsomes

Table 10. *In Vitro* Metabolic Stability Across Species for Compound 23

species	mouse	rat	dog	human
microsome Cl_{int} ($\mu\text{L}/\text{min}/\text{mg}$ protein)	<11.9	<11.9	5.8	<11.9
hepatocyte Cl_{int} ($\mu\text{L}/\text{min}/\text{million}$ cells)	n.d.	0.7	2.4	0.5

Table 11. *In Vivo* Pharmacokinetics of 23 in Rat and Dog

species	rat ^a		dog ^b	
route of administration	i.v.	p.o.	i.v.	p.o.
clearance (mL/min/kg)	4.5		13.7	
V_d (L/kg)	0.6		1.3	
$T_{1/2}$ (h)	2.8		1.5	
F (%)		94		39

^a $n = 3$ male SD rats, 2 mg/kg i.v., 10 mg/kg p.o. ^b $n = 2$ male Beagle dogs, 1 mg/kg i.v., 5 mg/kg p.o.

also target this important endonuclease in *L. donovani*. To test this hypothesis, we first assessed the potency of DNDI-6148 (23) against *T. brucei* bearing a mutation in the active site of CPSF3 (Asn²³²His), previously demonstrated to confer resistance to acoziborole (1).¹⁹ Bloodstream trypanosomes bearing this specific mutation were 1.8-fold less sensitive to DNDI-6148 (23) compared to wild-type parasites (Figure 2A). Similarly, trypanosomes overexpressing the wild-type version of CPSF3 were 2.9-fold less sensitive to DNDI-6148 (23) (Figure 2B). Collectively, these data suggest that, like acoziborole (1), this benzoxaborole specifically targets CPSF3 in *T. brucei*.

To determine if these boron-containing compounds specifically target CPSF3 in *L. donovani*, transgenic promastigotes were generated overexpressing either CPSF3^{WT} or CPSF3 bearing an Asn²¹⁹His mutation, equivalent to the Asn²³²His mutation in the *T. brucei* enzyme. Elevated levels of the wild-type and mutated CPSF3 in these cell lines were confirmed by label-free quantification (Figure S2). Overexpression of CPSF3^{WT} in *L. donovani* promastigotes did not substantively affect susceptibility to either acoziborole (1) (Figure 2C) or DNDI-6148 (23) (Figure 2D). However, promastigotes overexpressing the mutated version of this enzyme were significantly less sensitive to both compounds, demonstrating a 5-fold and 3.6-fold reduction in susceptibility to acoziborole (1) and DNDI-6148 (23), respectively (Figure 2C,D). The shift in potency observed with parasites overexpressing mutated CPSF3 was found to be specific for benzoxaboroles. Compound 3 elicited a similar shift in potency, while the established *N*-myristoyltransferase inhibitor

DDD100097²² did not (Figure S3). The fact that this single Asn²¹⁹His mutation in the active site of CPSF3 has a marked effect on the potencies of both acoziborole (1) and DNDI-6148 (23) provides strong evidence that this endonuclease is the molecular target of this preclinical candidate.

Precision Base Editing of *LdCPSF3*. We next utilized precision base editing with Cas9 to further probe the interactions between DNDI-6148 (23) and *L. donovani* CPSF3. In the first instance, a template encoding a specific Asn²¹⁹His mutation was provided to repair a Cas9-induced lesion within CPSF3. Transfected parasites were then selected with DNDI-6148 (23) (6 μM). The resulting DNDI-6148-resistant population was subcloned, genomic DNA was harvested, and the CPSF3 was sequenced to ensure that the desired edit had been successfully introduced. In all cases, these parasites maintained the Asn²¹⁹His encoded by the repair template and were consistently 3-fold less sensitive to DNDI-6148 (23) than wild-type (Table S2). As in our previous studies with *T. brucei* CPSF3, attempts to edit Asn²¹⁹ to Tyr to mimic the human CPSF3 enzyme at this position were not tolerated by *L. donovani*. However, using a degenerate repair template, parasites were recovered, maintaining Asn²¹⁹His and also Glu²²⁹Val homozygous mutations. These doubly mutated parasites were >5-fold less sensitive to DNDI-6148 (23) (Table S2). Collectively, these data provide compelling evidence that DNDI-6148 specifically targets the endonuclease CPSF3 in *L. donovani*. These data are also consistent with a recently published study reporting CPSF3 as amongst the top “hits” following the selection of the Cos-Seq genome-wide overexpression library with DNDI-6148.²³

Molecular Modeling. A homology model of the *L. donovani* CPSF3 was generated using the crystallographic structure of the *Thermus thermophilus* TTHA0252 homologue as a template (PDB code 3IEM—Figure 3). The *Leishmania* enzyme shares 30% sequence identity with this bacterial homologue. The proposed binding mode for DNDI-6148 (23) in the model is consistent with the binding of the benzoxaborole acoziborole to the catalytic site of CPSF3 located at the interface of the metallo- β -lactamase and β -CASP domains in *T. brucei* CPSF3.¹⁹ The site comprises two zinc atoms coordinated by a network of conserved histidine and aspartic acid residues. Interaction with a zinc-activated water molecule leads to the formation of a negatively charged tetrahedral boronate species that coordinates the zinc atoms (Figure S4), mimicking the transition state of the phosphate of the RNA substrate. The amide in position 6 of the benzoxaborole moiety directs the pyridyl-triazole moiety of

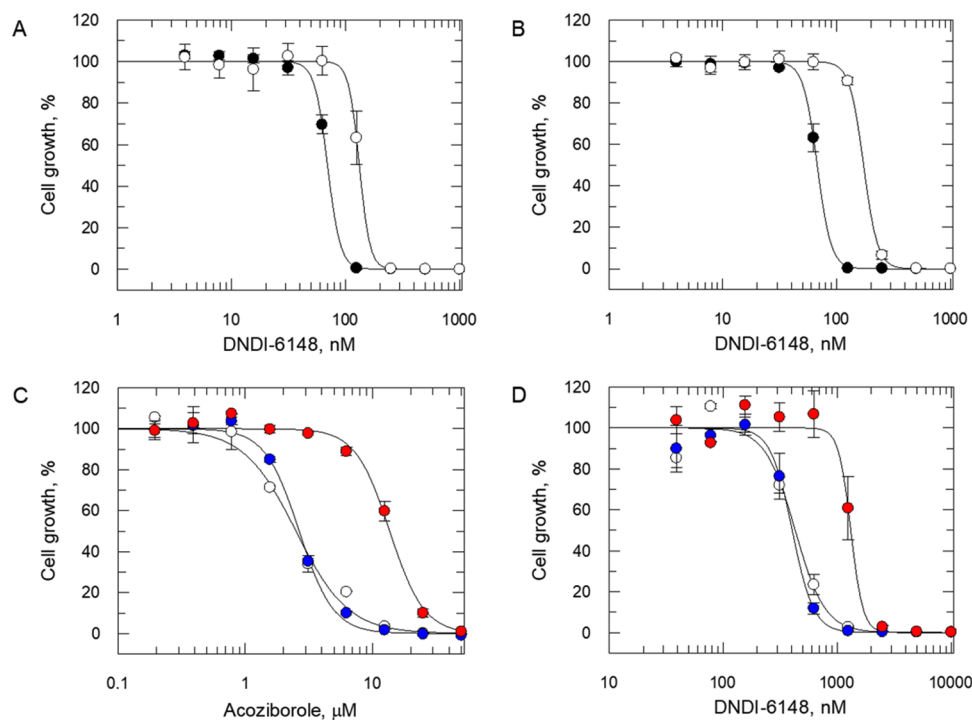


Figure 2. Potency of DNDI-6148 (**23**) against wild-type and transgenic *T. brucei* and *L. donovani*. (A) EC_{50} values for DNDI-6148 (**23**) were determined for wild-type *T. brucei* trypanosomes (closed circles) and *T. brucei* trypanosomes maintaining a mutated version of CPSF3 (Asn²³²His) (open circles). EC_{50} values of 47 ± 0.9 and 90 ± 3.4 nM were determined for wild-type and transgenic trypanosomes, respectively. (B) EC_{50} values of 67 ± 1 and 172 ± 3 nM were determined for DNDI-6148-treated wild-type trypanosomes (closed circles) and trypanosomes overexpressing the wild-type version of CPSF3, respectively. (C) EC_{50} values of 2.5 ± 0.1 , 2.8 ± 0.1 , and 11.7 ± 0.4 μ M were determined for acoziborole-treated wild-type (open circles), CPSF3-overexpressing (blue circles), and CPSF3 (Asn²¹⁹His)-overexpressing (red circles) *L. donovani* promastigotes, respectively. (D) EC_{50} values of 411 ± 12 , 508 ± 13 , and 1674 ± 51 nM were determined for DNDI-6148-treated wild-type (open circles), CPSF3-overexpressing (blue circles), and CPSF3 (Asn²¹⁹His)-overexpressing (red circles) *L. donovani* promastigotes, respectively. All curves are the nonlinear fits of data using a two-parameter EC_{50} equation provided by GraFit. EC_{50} values are the weighted mean \pm standard deviation of at three biological replicates ($n = 3$), with each biological replicate comprised of three technical replicates.

DNDI-6148 (**23**) toward the area occupied by the terminal uracil base of the RNA substrate and establishes a π -stacking interaction with Tyr³⁷⁰ (Figure 3A). Additionally, the amide NH forms a hydrogen bond with the hydroxyl group in the Thr²¹⁸ side-chain. There seems to be no direct interaction between DNDI-6148 (**23**) and the Asn²¹⁹ residue, where mutation to His is associated with resistance (Figure 3B). However, we propose that mutation to a bulkier His residue in this position has a negative impact on DNDI-6148 (**23**) binding due to steric clashes with the methyl pyridyl-triazole moiety of the compound (Figure 3C). This likely prompts the ligand to adopt a different binding mode where a hydrogen bond with Thr²¹⁸ is lost, the hydrophobic methyl is directed toward the solvent, and the overall ligand conformation is strained. Undoubtedly, there is a high degree of similarity surrounding the proposed binding site of DNDI-6148 in the parasite enzyme and the human homologue, with 21 identical residues out of the 26 within 5 Å from the bound ligand.¹⁹ However, Asn²¹⁹ in the parasite enzyme is replaced by a tyrosine residue in the human homologue. This bulkier tyrosine residue is likely to cause severe steric hindrance that prevents DNDI-6148 from binding to the human and is entirely consistent with the favorable selective toxicity profile of this compound.

The second mutation (Glu²²⁹Val) is at the beginning of helix 7 in the β -CASP domain of CPSF3. Helix 7 is some way from the catalytic site but is connected to the loop that contains Thr²¹⁸, Asn²¹⁹, and Ile²²¹, defining the pocket that recognizes

the pyridine ring of DNDI-6148 (**23**). In our models, a mutation from Glu²²⁹ to Val would result in a structural rearrangement of the loop, changing the morphology of the binding site and ultimately impacting the ligand recognition event.

CONCLUSIONS

We have optimized a series of benzoxaboroles and identified a range of compounds with very potent *in vitro* antileishmanial activity against *L. infantum* and *L. donovani*, starting from benzamide-substituted compound **3**. Variation of the amide substituent was explored extensively, and a range of heterocyclic amide groups was found to deliver potent *in vitro* activity combined with good metabolic stability. Several compounds were assessed in the *L. infantum* hamster model of VL, with compound **23** standing out by exhibiting very high levels of efficacy in all organs at doses of 25 mg/kg BID for 5 or 10 days. Additional *in vivo* studies in the *L. donovani* hamster model also indicated high levels of efficacy, demonstrating that **23** was equally efficacious against both *Leishmania* species responsible for causing VL. Efficacy of **23** was also confirmed in *L. donovani* and *L. infantum* BALB/c mouse models. Further study of compound **23** indicated that it had excellent pharmacokinetics, a good *in vitro* safety profile, and met all of the criteria in the DNDi TCP for VL. Comprehensive MoA studies confirm that DNDI-6148 (**23**) targets the endonuclease CPSF3, a previously unexploited drug target in *Leishmania* spp. Consequently, **23** (DNDI-6148) was

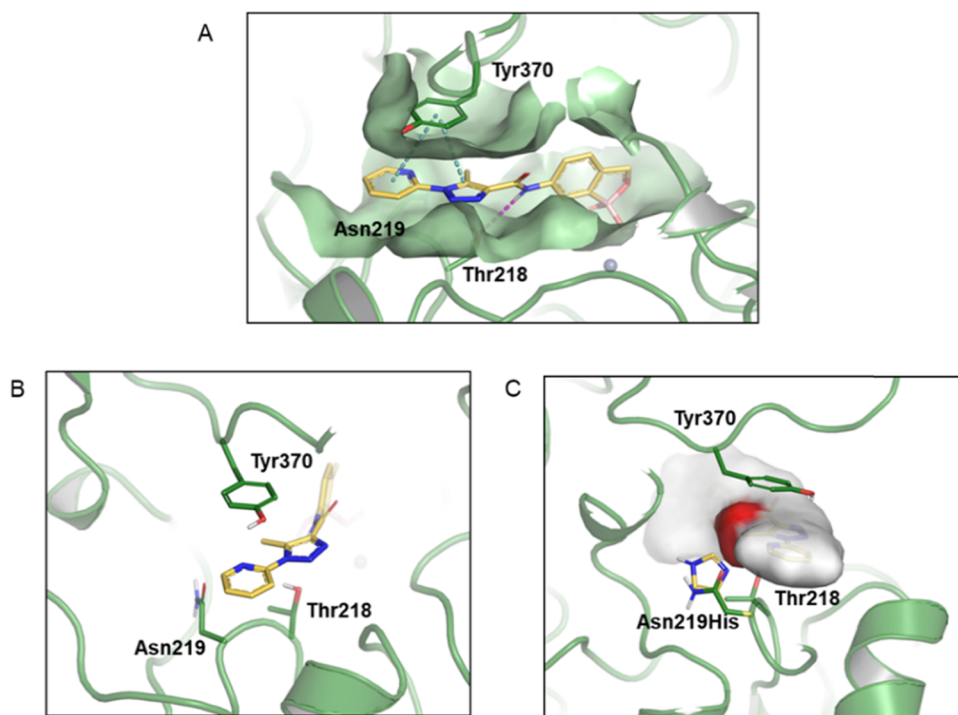


Figure 3. Molecular docking of DNDI-6148 into a model of the *L. donovani* CPSF3 active site. (A) Docking model for DNDI-6148 (**23**) (yellow structure) bound to *L. donovani* CPSF3. Gray spheres represent zinc atoms, blue dotted lines indicate a π stacking interaction, and the purple dotted line indicates a hydrogen bond interaction. (B) Close-up of key interactions involved in DNDI-6148 (**23**) (yellow structure) binding in the active site of CPSF3. (C) Modified docking model illustrating a steric clash between DNDI-6148 (**23**) (red patch) and the His residue (yellow) in Asn²¹⁹His substituted CPSF3. The wild-type CPSF3 structure is shown in green.

nominated as a preclinical candidate and further development toward clinical studies is ongoing. Furthermore, compound **23** demonstrates similar levels of *in vitro* and *in vivo* activity against species of *Leishmania* responsible for causing cutaneous leishmaniasis (CL), supporting the development of this candidate for multiple forms of leishmaniasis.²⁴ It should be noted that we have also generated data that supports the development of DNDI-6148 for Chagas' disease. This information will be disclosed in due course. In conclusion, the data package for DNDI-6148 (**23**) provides every reason to believe that this benzoxaborole can become a much-needed safe oral treatment for patients suffering from this devastating neglected tropical disease.

EXPERIMENTAL SECTION

Chemistry. Purity. All compounds reported in this study are >95% pure as determined by high-performance liquid chromatography (HPLC) analysis. HPLC chromatograms of a representative compound (**3**) and all analogues used in *in vivo* experiments (**5**, **16**, **23**, **28**, **31**) are shown in the Supplementary Information (Figures S6–S11).

General. Unless otherwise indicated, all reactions were magnetically stirred under an inert atmosphere. All reagents, including solvents, were used as received. Anhydrous solvents were dried in-house by passing through activated alumina. Thin-layer chromatography was performed on glass-backed precoated silica gel 60 plates, and compounds were visualized using UV light or iodine. Silica gel column chromatography was performed using 200–300-mesh silica gel. Preparative HPLC was performed using Gilson-281 liquid handlers equipped with one of four columns, chosen from (1) Phenomenex Synergi C18 150 mm \times 30 mm, 4 μ m, (2) YMC-pack ODS-AQ 150 mm \times 30 mm, 5 μ m, (3) Agela Venusil ASB C18 150 mm \times 21.2 mm, 5 μ m, or (4) Boston Symmetrix C18 ODS-R 150 mm \times 30 mm, 5 μ m; elution was performed with 0.225% (by

volume) of formic acid in water (solvent A) and acetonitrile (solvent B); fractions containing products were lyophilized. NMR spectra were recorded on a Bruker AVANCE 400 MHz spectrometer in the solvents specified. Liquid chromatography–mass spectrometry (LC-MS) spectra were recorded on an Agilent 1200 or Shimadzu 2020 spectrometer equipped with electrospray ionization, quadrupole MS detector, and Chromolith Flash RP-18e 25 mm \times 2.0 mm column, eluting with 0.0375% (by volume) of trifluoroacetic acid (TFA) in water (solvent A) and 0.01875% (by volume) of TFA in acetonitrile (solvent B). Analytical HPLC was performed using a Shimadzu LC20AB machine and one of two columns, chosen from (1) Xtimate C18 2.1 mm \times 30 mm, 3 μ m or (2) CHROM-MATRIX Innovation C18 2.1 mm \times 30 mm, 2.6 μ m; elution was performed with 0.0375% (by volume) of TFA in water (solvent A) and 0.01875% (by volume) of TFA in acetonitrile (solvent B). The purity of final compounds was \geq 96%, as determined by HPLC. Unless otherwise stated, final compounds were isolated as amorphous solids without collection of melting point data.

General Procedures for the Preparation of Amides. General Procedure A. To a solution of the corresponding acid (14.4 mmol, 1.0 equiv), HOBt (17.3 mmol, 1.2 equiv), EDCI (17.3 mmol, 1.2 equiv), and DIPEA (36.1, 2.5 equiv) in dichloromethane (DCM) (30 mL) was added 6-aminobenzo[*c*][1,2]oxaborol-1(3*H*)-ol (14.4 mmol, 1.0 equiv). The reaction mixture was stirred at room temperature for 2 h. Water (100 mL) was added, and the reaction mixture was extracted with DCM (100 mL \times 3). The combined organic extracts were washed with brine (100 mL \times 2), dried with anhydrous Na₂SO₄, filtered, and concentrated in a vacuum to give the crude product, which was purified by silica gel chromatography or preparative HPLC.

General Procedure B. To a solution of the corresponding acid (1.5 mmol, 1.0 equiv), HATU (1.9 mmol, 1.3 equiv), and DIPEA (2.8 mmol, 1.8 equiv) in DMF (3 mL) was added 6-aminobenzo[*c*][1,2]-oxaborol-1(3*H*)-ol (1.5 mmol, 1.0 equiv). The mixture was stirred at room temperature overnight. The mixture was purified by preparative HPLC.

General Procedure C. A solution of the corresponding acid (10.5 mmol) in SOCl_2 (40 mL) was stirred at 50 °C for 4 h. The mixture was concentrated in a vacuum to give acyl chloride, which was used directly in the next step. To a solution of 6-aminobenzo[*c*][1,2]-oxaborol-1(3*H*)-ol (1.2 g, 8.1 mmol) and DIPEA (2.9 mL, 16.7 mmol) in THF (30 mL) was added the acid chloride (8.1 mmol). The mixture was stirred at room temperature for 16 h. Water (100 mL) was added, and the reaction mixture was extracted with EtOAc (100 mL × 3). The combined organic extracts were washed with brine (100 mL × 2), dried with anhydrous Na_2SO_4 , filtered, and concentrated in a vacuum to give the crude product, which was purified by silica gel chromatography or preparative HPLC.

***N*-(1-Hydroxy-1,3-dihydrobenzo[*c*][1,2]oxaborol-6-yl)-1,3-bis-(trifluoromethyl)-1*H*-pyrazole-4-carboxamide (4).** The title compound was synthesized according to method B using a mixture of 1,3-bis-(trifluoromethyl)-1*H*-pyrazole-4-carboxylic acid and 1,5-bis-(trifluoromethyl)-1*H*-pyrazole-4-carboxylic acid (4 g, 16 mmol), HATU (7.3 g, 19.2 mmol), 6-aminobenzo[*c*][1,2]oxaborol-1(3*H*)-ol 2 (2.9 g, 19.2 mmol), DIPEA (4.1 g, 32 mmol), and DMF (30 mL) to yield 6.5 g of crude product as a yellow solid. 2 g of the crude product was purified by prep-HPLC to yield 4 as a white solid (200 mg). HPLC: 100% pure. MS (ESI) $m/z = 380.1$ [$M + 1$]⁺. ¹H NMR (400 MHz, $\text{DMSO-}d_6$) $\delta = 10.54$ (s, 1H), 9.44 (s, 1H), 9.32 (brs, 1H), 8.18 (s, 1H), 7.65 (d, $J = 7.2$ Hz, 1H), 7.42 (d, $J = 8.4$ Hz, 1H), 4.98 (s, 2H). HRMS (ES⁺): calcd for $\text{C}_{13}\text{H}_9\text{B}_1\text{F}_6\text{N}_3\text{O}_3$ [$M + \text{H}$]⁺ 380.0641, found 380.0644 (0.75 ppm).

***N*-(1-Hydroxy-1,3-dihydrobenzo[*c*][1,2]oxaborol-6-yl)-1-(2,2,2-trifluoroethyl)-3-(trifluoromethyl)-1*H*-pyrazole-4-carboxamide (5).** To a cold solution of 6-amino-3,3-dimethylbenzo[*c*][1,2]oxaborol-1(3*H*)-ol 2 (22.7 g, 152.3 mmol) and DIPEA (39.3 g, 305.2 mmol) in THF (500 mL) was added a solution of 1-(2,2,2-trifluoroethyl)-3-(trifluoromethyl)-1*H*-pyrazole-4-carboxylic acid (42.7 g, 152.5 mmol) in THF (150 mL) dropwise. The mixture was stirred at room temperature for 4 h and concentrated in a vacuum to a residue that was recrystallized from MeCN and water to yield 5 as a gray solid (41.1 g, 68%). HPLC: 98% pure. MS (ESI) $m/z = 394.2$ [$M + \text{H}$]⁺. ¹H NMR (400 MHz, $\text{DMSO-}d_6$) $\delta = 10.37$ (s, 1H), 9.27 (s, 1H), 8.72 (s, 1H), 8.16 (s, 1H), 7.66 (dd, $J = 2.0, 8.0$ Hz, 1H), 7.39 (d, $J = 8.4$ Hz, 1H), 5.48 (q, $J = 9.2$ Hz, 2H), 4.97 (s, 2H).

***N*-(1-Hydroxy-1,3-dihydrobenzo[*c*][1,2]oxaborol-6-yl)-3-(trifluoromethyl)-1-(3,3,3-trifluoropropyl)-1*H*-pyrazole-4-carboxamide (6).** The title compound was synthesized according to method B using 3-(trifluoromethyl)-1-(3,3,3-trifluoropropyl)pyrazole-4-carboxylic acid 6 (18.0 g, 65.2 mmol), HATU (34.7 g, 91.3 mmol), 1-hydroxy-3*H*-2,1-benzoxaborol-6-amine 2 (10.7 g, 71.8 mmol), DIPEA (16.9 g, 131.0 mmol), and DMF (150 mL) to give a residue. The residue was purified by silica gel chromatography (elution with ethyl acetate/petroleum ether/AcOH = 1: 3: 0.1) to give the crude product, which was recrystallized from MeOH to yield 6 as a white solid (9.60 g, 36.2%). HPLC: 99% pure. MS (ESI) $m/z = 408.1$ [$M + 1$]⁺. ¹H NMR (400 MHz, $\text{DMSO-}d_6$) $\delta = 10.22$ (s, 1H), 9.25 (s, 1H), 8.66 (s, 1H), 8.17 (s, 1H), 7.64 (d, $J = 8.0$ Hz, 1H), 7.38 (d, $J = 8.0$ Hz, 1H), 4.96 (s, 2H), 4.56 (t, $J = 6.8$ Hz, 2H), 3.02 (m, 2H). HRMS (ES⁺): calcd for $\text{C}_{15}\text{H}_{13}\text{B}_1\text{F}_6\text{N}_3\text{O}_3$ [$M + \text{H}$]⁺ 408.0954, found 408.0957 (0.70 ppm).

***N*-(1-Hydroxy-1,3-dihydrobenzo[*c*][1,2]oxaborol-6-yl)-3-methyl-1-(3,3,3-trifluoropropyl)-1*H*-pyrazole-4-carboxamide (7) and *N*-(1-Hydroxy-1,3-dihydrobenzo[*c*][1,2]oxaborol-6-yl)-5-methyl-1-(3,3,3-trifluoropropyl)-1*H*-pyrazole-4-carboxamide (15).** The title compounds were synthesized according to method B using a mixture of 3-methyl-1-(3,3,3-trifluoropropyl)-1*H*-pyrazole-4-carboxylic acid and 5-methyl-1-(3,3,3-trifluoropropyl)-1*H*-pyrazole-4-carboxylic acid (469 mg, 2.1 mmol), HATU (890 mg, 2.3 mmol), 6-aminobenzo[*c*][1,2]-oxaborol-1(3*H*)-ol 2 (300 mg, 2.0 mmol), HATU (890 mg, 2.3 mmol), DIPEA (520 mg, 4.0 mmol), and DMF (5 mL) to yield the crude product, which was purified by preparative HPLC to give 7 (207 mg, 29%) as a white solid and 15 (205 mg, 29%) as a white solid.

7: HPLC: 99% pure. MS (ESI) $m/z = 354$ [$M + \text{H}$]⁺. ¹H NMR (400 MHz, $\text{DMSO-}d_6$) $\delta = 9.77$ (s, 1H), 9.21 (s, 1H), 8.42 (s, 1H), 8.14 (s, 1H), 7.68 (d, $J = 8.0$ Hz, 1H), 7.36 (d, $J = 8.0$ Hz, 1H), 4.97 (s,

2H), 4.38 (t, $J = 6.8$ Hz, 2H), 2.90 (m, 2H), 2.40 (s, 3H). HRMS (ES⁺): calcd for $\text{C}_{15}\text{H}_{16}\text{B}_1\text{F}_3\text{N}_3\text{O}_3$ [$M + \text{H}$]⁺ 354.1237, found 354.1240 (0.90 ppm).

15: HPLC: 99% pure. MS (ESI) $m/z = 354$ [$M + \text{H}$]⁺. ¹H NMR (400 MHz, $\text{DMSO-}d_6$) $\delta = 9.79$ (s, 1H), 9.22 (s, 1H), 8.16 (s, 1H), 8.12 (s, 1H), 7.79 (d, $J = 8.4$ Hz, 1H), 7.36 (d, $J = 8.4$ Hz, 1H), 4.96 (s, 2H), 4.35 (t, $J = 6.8$ Hz, 2H), 2.87 (m, 2H), 2.57 (s, 3H). HRMS (ES⁺): calcd for $\text{C}_{15}\text{H}_{16}\text{B}_1\text{F}_3\text{N}_3\text{O}_3$ [$M + \text{H}$]⁺ 354.1237, found 354.1240 (0.90 ppm).

Cyclobutyl-*N*-(1-hydroxy-1,3-dihydrobenzo[*c*][1,2]oxaborol-6-yl)-3-methyl-1*H*-pyrazole-4-carboxamide (8). The title compound was synthesized according to method B using cyclobutyl-3-methyl-1*H*-pyrazole-4-carboxylic acid (201.0 mg, 1.1 mmol), 6-aminobenzo[*c*][1,2]oxaborol-1(3*H*)-ol 2 (167.0 mg, 1.1 mmol), HATU (543.0 mg, 1.4 mmol), DIPEA (180.0 mg, 1.4 mmol), and DMF (8 mL) to yield the crude product, which was purified by preparative HPLC to yield 8 as a white solid (96.6 mg, 28%). HPLC: 99% pure. MS (ESI) $m/z = 312.1$ [$M + \text{H}$]⁺. ¹H NMR (400 MHz, $\text{DMSO-}d_6$) $\delta = 9.71$ (s, 1H), 9.21 (s, 1H), 8.43 (s, 1H), 8.12 (d, $J = 1.6$ Hz, 1H), 7.67 (dd, $J = 8.4, 2.0$ Hz, 1H), 7.35 (d, $J = 8.4$ Hz, 1H), 4.96 (s, 2H), 4.80 (m, 1H), 2.40 (m, 7H), 1.82 (m, 2H). HRMS (ES⁺): calcd for $\text{C}_{16}\text{H}_{19}\text{B}_1\text{N}_3\text{O}_3$ [$M + \text{H}$]⁺ 312.1519, found 312.1523 (1.13 ppm).

1-Cyclobutyl-*N*-(1-hydroxy-1,3-dihydrobenzo[*c*][1,2]oxaborol-6-yl)-3-(trifluoromethyl)-1*H*-pyrazole-4-carboxamide (9). The title compound was synthesized according to method B using 1-cyclobutyl-3-(trifluoromethyl)-1*H*-pyrazole-4-carboxylic acid (565 mg, 2.4 mmol), HATU (1.2 g, 3.2 mmol), 6-aminobenzo[*c*][1,2]-oxaborol-1(3*H*)-ol 2 (430.0 mg, 2.9 mmol), DIPEA (805.0 mg, 6.2 mmol), and DMF (4 mL) to yield the crude product, which was purified by preparative HPLC to yield 9 as a white solid (278.0 mg, 32%). HPLC: 100% pure. MS (ESI) $m/z = 366.0$ [$M + 1$]⁺. ¹H NMR (400 MHz, $\text{DMSO-}d_6$) $\delta = 10.16$ (s, 1H), 9.25 (s, 1H), 8.68 (s, 1H), 8.16 (s, 1H), 7.63 (dd, $J = 1.6, 8.0$ Hz, 1H), 7.38 (d, $J = 8.4$ Hz, 1H), 4.99 (m, 1H), 4.96 (s, 2H), 2.47 (m, 4H), 1.86 (m, 2H). HRMS (ES⁺): calcd for $\text{C}_{16}\text{H}_{16}\text{B}_1\text{F}_3\text{N}_3\text{O}_3$ [$M + \text{H}$]⁺ 366.1237, found 366.1240 (0.87 ppm).

***N*-(1-Hydroxy-1,3-dihydrobenzo[*c*][1,2]oxaborol-6-yl)-1-(tetrahydro-2*H*-pyran-4-yl)-3-(trifluoromethyl)-1*H*-pyrazole-4-carboxamide (10).** The title compound was synthesized according to method B using 1-(tetrahydro-2*H*-pyran-4-yl)-3-(trifluoromethyl)-1*H*-pyrazole-4-carboxylic acid (900 mg, 3.4 mmol), HATU (1.9 g, 5.1 mmol), 6-aminobenzo[*c*][1,2]oxaborol-1(3*H*)-ol 2 (507 mg, 3.4 mmol), and DIPEA (880 mg, 6.8 mmol) to yield the crude product, which was purified by preparative HPLC to yield 10 as a pink solid (358.6 mg, 26.7%). HPLC: 100% pure. MS (ESI) $m/z = 396.0$ [$M + 1$]⁺. ¹H NMR (400 MHz, $\text{DMSO-}d_6$) $\delta = 10.16$ (s, 1H), 9.26 (s, 1H), 8.68 (s, 1H), 8.16 (s, 1H), 7.63 (d, $J = 8.0$ Hz, 1H), 7.38 (d, $J = 8.0$ Hz, 1H), 4.96 (s, 2H), 4.58 (m, 1H), 4.00 (m, 2H), 3.50 (t, $J = 11.0$ Hz, 2H), 2.07 (m, 2H), 1.96 (m, 2H). HRMS (ES⁺): calcd for $\text{C}_{17}\text{H}_{18}\text{B}_1\text{Fe}_3\text{N}_3\text{O}_4$ [$M + \text{H}$]⁺ 396.1342, found 396.1346 (0.89 ppm).

***N*-(1-Hydroxy-1,3-dihydro-2,1-benzoxaborol-6-yl)-3-methyl-1-(pyridine-2-yl)-1*H*-pyrazole-4-carboxamide (11).** The title compound was synthesized according to method B using 3-methyl-1-(pyridin-2-yl)-1*H*-pyrazole-4-carboxylic acid (211 mg, 1.04 mmol), HATU (400 mg, 1.05 mmol), 6-aminobenzo[*c*][1,2]oxaborol-1(3*H*)-ol 2 (155 mg, 1.04 mmol), and DIPEA (0.27 mL, 1.56 mmol) to yield the crude product, which was triturated with DCM. The precipitated product was collected by filtration to give 11 (198 mg 54%) as an off-white solid. ¹H NMR ($\text{DMSO-}d_6$ with 0.05% v/v tetramethylsilane (TMS), 400 MHz): $\delta = 2.52$ (s, 3H, CH_3), 4.97 (s, 2H, CH_2), 7.37 (d, 1H, Ar, $J = 8.0$ Hz), 7.42 (ddd, 1H, ArH, $J = 7.6$ Hz, $J = 5.2$ Hz, $J = 1.2$ Hz), 7.73 (dd, ArH, $J = 8.4$ Hz, $J = 2.0$ Hz), 7.94 (d, 1H, ArH, $J = 8.0$ Hz), 8.03 (dd, 1H, ArH, $J = 8.0$ Hz, $J = 1.6$ Hz), 8.21 (d, 1H, ArH, $J = 2.0$ Hz), 8.54 (m, 1H, ArH), 9.47 (s, 1H, ArH), 9.70 (s, 1H, OH), 10.06 (s, 1H, NH).

6-(((1-(Pyridin-2-yl)-3-(trifluoromethyl)-1*H*-pyrazole-4-carbonyloxy)amino)benzo[*c*][1,2]oxaborol-1(3*H*)-ol (12). The title compound was synthesized according to method A using 1-(pyridin-2-yl)-3-(trifluoromethyl)-1*H*-pyrazole-4-carboxylic acid (200.0 mg, 0.78 mmol), 6-aminobenzo[*c*][1,2]oxaborol-1(3*H*)-ol 2 (120.0 mg, 0.8

mmol), HOBt (126.4 mg, 0.9 mmol), EDCI (172.8 mg, 0.9 mmol), DIPEA (201.0 mg, 1.6 mmol), and DMF (5 mL) to yield the crude product, which was purified by preparative HPLC to yield **12** as a white solid (200.0 mg, 66%). HPLC: 99% pure. MS (ESI) $m/z = 389$ $[M+H]^+$. 1H NMR (400 MHz, DMSO- d_6): δ 10.41 (s, 1H), 9.66 (s, 1H), 9.26 (s, 1H), 8.63 (m, 1H), 8.26 (d, $J = 1.6$ Hz, 1H), 8.15 (m, 1H), 8.04 (d, $J = 8.4$ Hz, 1H), 7.72 (dd, $J = 8.0, 2.0$ Hz, 1H), 7.58 (m, 1H), 7.40 (d, $J = 8.4$ Hz, 1H), 5.00 (s, 2H). HRMS (ES+): calcd for $C_{17}H_{13}B_1F_3N_4O_3$ $[M+H]^+$ 389.1033, found 389.1036 (0.82 ppm).

6-(((1-(4-Chlorophenyl)-3-(trifluoromethyl)-1H-pyrazole-4-carbonyloxy)amino)benzo[*c*][1,2]oxaborol-1(3H)-ol (**13**)). The title compound was synthesized according to method B using 1-(4-chlorophenyl)-3-(trifluoromethyl)-1H-pyrazole-4-carboxylic acid (200 mg, 0.7 mmol), 6-aminobenzo[*c*][1,2]oxaborol-1(3H)-ol **2** (134 mg, 0.9 mmol), HATU (315.0 mg, 0.83 mmol), HATU (315.0 mg, 0.83 mmol), TEA (0.2 mL, 1.4 mmol), and DMF (5 mL) to yield the crude product, which was purified by preparative HPLC to yield **13** as a white solid (180.0 mg, 62%). HPLC: 99% pure. MS (ESI) $m/z = 422.0$ $[M+H]^+$. 1H NMR (400 MHz, DMSO- d_6): δ 10.32 (s, 1H), 9.32 (s, 1H), 9.26 (s, 1H), 8.19 (s, 1H), 7.92 (d, $J = 8.8$ Hz, 2H), 7.68 (m, 3H), 7.41 (d, $J = 8.0$ Hz, 1H), 4.98 (s, 2H).

N-(1-Hydroxy-1,3-dihydro-2,1-benzoxaborol-6-yl)-1-(2-methoxyphenyl)-3-methyl-1H-pyrazole-4-carboxamide (**14**). The title compound was synthesized according to method B using 1-(2-methoxyphenyl)-3-methyl-1H-pyrazole-4-carboxylic acid (300 mg, 1.29 mmol), 6-aminobenzo[*c*][1,2]oxaborol-1(3H)-ol **2** (192 mg, 1.29 mmol), HATU (491 mg, 1.29 mmol), DIPEA (250 mg, 1.94 mmol), and DMF (3 mL) to yield the crude product, which was triturated with DCM. The precipitated product was collected by filtration and recrystallized from $CHCl_3$ to give **14** (190 mg, 41%) as an off-white solid. 1H NMR ($CDCl_3$ with 0.05% v/v TMS, 400 MHz): δ 2.50 (s, 3H, CH_3), 3.93 (s, 3H, CH_3), 4.97 (s, 2H, CH_2), 7.09–7.14 (m, 1H, ArH), 7.29–7.32 (m, 1H, ArH), 7.36–7.43 (m, 2H, ArH), 7.67–7.72 (m, 2H, ArH), 8.14 (d, 1H, ArH, $J = 1.6$ Hz), 8.88 (s, 1H, ArH), 9.23 (s, 1H, OH), 9.89 (s, 1H, NH).

N-(1-Hydroxy-1,3-dihydrobenzo[*c*][1,2]oxaborol-6-yl)-5-methyl-1-(pyridin-2-yl)-1H-pyrazole-4-carboxamide (**16**). A solution of 5-methyl-1-(pyridin-2-yl)-1H-pyrazole-4-carboxylic acid (15.0 g, 73.9 mmol) in $SOCl_2$ (100 mL) was stirred at 50 °C for 4 h. The mixture was concentrated in a vacuum to give acyl chloride, which was used directly in the next step. To a solution of 6-aminobenzo[*c*][1,2]oxaborol-1(3H)-ol **2** (11.0 g, 73.8 mmol) and DIPEA (15 mL) in DCM (30 mL) was added a solution of acyl chloride in DCM (20 mL) dropwise at 0 °C. The mixture was stirred at room temperature for 1 h. The precipitate was filtered and the cake was washed with MTBE (100 mL) and water (50 mL), dried in a vacuum and recrystallized from THF (50 mL) to yield **16** as a white solid (16.0 g, 65%). HPLC: 100% pure. MS (ESI) $m/z = 335.2$ $[M+H]^+$. 1H NMR (400 MHz, DMSO- d_6): δ 9.99 (s, 1H), 9.24 (s, 1H), 8.57 (dd, $J = 5.2, 1.2$ Hz, 1H), 8.36 (s, 1H), 8.14 (d, $J = 1.6$ Hz, 1H), 8.07 (m, 1H), 7.84 (d, $J = 8.0$ Hz, 1H), 7.72 (m, 1H), 7.40 (m, 1H), 7.37 (d, $J = 8.4$ Hz, 1H), 4.98 (s, 2H), 2.85 (s, 3H).

N-(1-Hydroxy-1,3-dihydrobenzo[*c*][1,2]oxaborol-6-yl)-1-(6-methoxypyridin-2-yl)-5-methyl-1H-pyrazole-4-carboxamide (**17**). The title compound was synthesized according to method B using 1-(6-methoxypyridin-2-yl)-5-methyl-1H-pyrazole-4-carboxylic acid (2.3 g, 10 mmol), 6-aminobenzo[*c*][1,2]oxaborol-1(3H)-ol **2** (1.50 g, 10 mmol), HATU (3.8 g, 10 mmol), DIPEA (3.9 g, 30 mmol), and DMF (20 mL) to yield the crude product, which was purified by preparative HPLC to yield **17** as a white solid (2.8 g, 77%). HPLC: 99% pure. MS (ESI) $m/z = 365.0$ $[M+H]^+$. 1H NMR (400 MHz, DMSO- d_6): δ 9.97 (s, 1H), 9.22 (s, 1H), 8.34 (s, 1H), 8.16 (d, $J = 1.6$ Hz, 1H), 7.94 (t, $J = 8.0$ Hz, 1H), 7.73 (dd, $J = 8.0, 2.0$ Hz, 1H), 7.45 (d, $J = 7.6$ Hz, 1H), 7.39 (d, $J = 8.4$ Hz, 1H), 6.88 (d, $J = 8.0$ Hz, 1H), 4.98 (s, 2H), 3.93 (s, 3H), 2.94 (s, 3H). HRMS (ES+): calcd for $C_{18}H_{18}B_1N_4O_4$ $[M+H]^+$ 365.1421, found 365.1425 (1.07 ppm).

N-(1-Hydroxy-1,3-dihydrobenzo[*c*][1,2]oxaborol-6-yl)-5-methyl-1-(6-methylpyridin-2-yl)-1H-pyrazole-4-carboxamide (**18**). The title compound was synthesized according to method B using 5-methyl-1-(6-methylpyridin-2-yl)-1H-pyrazole-4-carboxylic acid (100.0 mg, 0.5

mmol), 6-aminobenzo[*c*][1,2]oxaborol-1(3H)-ol **2** (82.0 mg, 0.5 mmol), HATU (210 mg, 0.6 mmol), DIPEA (89 mg, 0.7 mmol), and DMF (3 mL) to yield the crude product, which was purified by preparative HPLC to yield **18** as a white solid (34.8 mg, 22%). HPLC: 96% pure. MS (ESI) $m/z = 349.1$ $[M + 1]^+$. 1H NMR (400 MHz, DMSO- d_6): δ 9.95 (s, 1H), 9.21 (s, 1H), 8.33 (s, 1H), 8.15 (s, 1H), 7.92 (t, $J = 7.6$ Hz, 1H), 7.72 (d, $J = 10.0$ Hz, 1H), 7.61 (d, $J = 8.0$ Hz, 1H), 7.35 (m, 2H), 4.97 (s, 2H), 2.84 (s, 3H), 2.54 (s, 3H).

N-(1-Hydroxy-1,3-dihydrobenzo[*c*][1,2]oxaborol-6-yl)-3-(pyridin-2-yl)-1H-pyrazole-5-carboxamide (**19**). To a solution of 6-aminobenzo[*c*][1,2]oxaborol-1(3H)-ol **2** (357.0 mg, 2.4 mmol) and DIPEA (619.0 mg, 4.8 mmol) in MeCN (10 mL) was added a solution of 3-(pyridin-2-yl)-1H-pyrazole-5-carbonyl chloride (500 mg, 2.4 mmol) in MeCN (10 mL) dropwise. The mixture was stirred at 60 °C for 20 h. The mixture was concentrated in a vacuum to give a crude product, which was purified by preparative HPLC to yield **19** as a white solid (28.4 mg, 3.7%). HPLC: 96% pure. MS (ESI) $m/z = 321.1$ $[M + 1]^+$. 1H NMR (400 MHz, DMSO- d_6): δ 8.65 (d, $J = 4.4$ Hz, 1H), 8.21 (s, 1H), 8.01 (d, $J = 8.0$ Hz, 1H), 7.90 (t, $J = 7.8$ Hz, 1H), 7.82 (dd, $J = 2.0, 8.0$ Hz, 1H), 7.51 (s, 1H), 7.38 (m, 2H), 4.98 (s, 2H).

N-(1-Hydroxy-1,3-dihydrobenzo[*c*][1,2]oxaborol-6-yl)-1-methyl-3-(pyridin-2-yl)-1H-pyrazole-5-carboxamide (**20**) and *N*-(1-Hydroxy-1,3-dihydrobenzo[*c*][1,2]oxaborol-6-yl)-1-methyl-5-(pyridin-2-yl)-1H-pyrazole-3-carboxamide (**21**). The title compounds were synthesized according to method B using a mixture of 1-methyl-3-(pyridin-2-yl)-1H-pyrazole-5-carboxylic acid and 1-methyl-5-(pyridin-2-yl)-1H-pyrazole-3-carboxylic acid (300 mg, 1.5 mmol), HATU (722 mg, 1.9 mmol), 6-aminobenzo[*c*][1,2]oxaborol-1(3H)-ol **2** (222.0 mg, 1.5 mmol), DIPEA (361.0 mg, 2.8 mmol), and DMF (3 mL) to yield the crude product, which was purified by preparative HPLC to give **20** (123 mg, 25%) as a white solid and **21** (40.7 mg, 8%) as a white solid.

20: HPLC: 99% pure. LC-MS (ESI) $m/z = 335.1$ $[M + 1]^+$, $t = 0.931$ min. 1H NMR (400 MHz, DMSO- d_6): δ 10.42 (s, 1H), 9.29 (s, 1H), 8.63 (d, $J = 4.4$ Hz, 1H), 8.23 (s, 1H), 7.97 (d, $J = 8.0$ Hz, 1H), 7.87 (m, 1H), 7.78 (m, 2H), 7.41 (d, $J = 8.0$ Hz, 1H), 7.37 (m, 1H), 4.98 (s, 2H), 4.20 (s, 3H). HRMS (ES+): calcd for $C_{17}H_{16}B_1N_4O_3$ $[M+H]^+$ 335.1315, found 335.1319 (1.06 ppm).

21: HPLC: 99% pure. LC-MS (ESI) $m/z = 335.1$ $[M + 1]^+$, $t = 1.026$ min. 1H NMR (400 MHz, DMSO- d_6): δ 10.18 (s, 1H), 9.26 (s, 1H), 8.73 (d, $J = 4.8$ Hz, 1H), 8.23 (s, 1H), 7.95 (m, 2H), 7.80 (d, $J = 6.8$ Hz, 1H), 7.45 (m, 1H), 7.36 (m, 2H), 4.97 (s, 2H), 4.28 (s, 3H). HRMS (ES+): calcd for $C_{17}H_{16}B_1N_4O_3$ $[M+H]^+$ 335.1315, found 335.1319 (1.06 ppm).

N-(1-Hydroxy-1,3-dihydrobenzo[*c*][1,2]oxaborol-6-yl)-1-(pyridin-2-yl)-1H-1,2,3-triazole-4-carboxamide (**22**). To a solution of 6-amino-3,3-dimethylbenzo[*c*][1,2]oxaborol-1(3H)-ol **2** (1.6 g, 10.5 mmol) and DIPEA (2.7 g, 21.0 mmol) in THF (20 mL) was added a solution of 1-(pyridin-2-yl)-1H-1,2,3-triazole-4-carbonyl chloride (2.2 g, 10.5 mmol) in THF (80 mL) at 0 °C. The mixture was stirred at room temperature for 4 h. The solvent was removed in a vacuum and the residue was recrystallized with MeCN and water to yield **22** as a gray solid (1.7 g, 51%). HPLC: 100% pure. MS (ESI) $m/z = 321.9$ $[M+H]^+$. 1H NMR (400 MHz, DMSO- d_6): δ 10.61 (s, 1H), 9.39 (s, 1H), 9.27 (s, 1H), 8.67 (d, $J = 4.4$ Hz, 1H), 8.20 (m, 3H), 7.82 (dd, $J = 8.8, 2.0$ Hz, 1H), 7.63 (m, 1H), 7.41 (d, $J = 8.4$ Hz, 1H), 4.98 (s, 2H). HRMS (ES+): calcd for $C_{15}H_{12}B_1N_5O_3Na_1$ $[M+Na]^+$ 344.0931, found 344.0934 (0.90 ppm).

N-(1-Hydroxy-1,3-dihydrobenzo[*c*][1,2]oxaborol-6-yl)-5-methyl-1-(pyridin-2-yl)-1H-1,2,3-triazole-4-carboxamide (**23**). The title compound was synthesized according to method B using 5-methyl-1-(pyridin-2-yl)-1H-1,2,3-triazole-4-carboxylic acid (3.3 g, 16.2 mmol), 6-aminobenzo[*c*][1,2]oxaborol-1(3H)-ol **2** (2.9 g, 19.4 mmol), HATU (8.0 g, 21.0 mmol), DIPEA (4.2 g, 32.3 mmol), and DMF (30 mL) to yield the crude product, which was purified by preparative HPLC to yield **23** as a yellow solid (4.0 g, 74.1%). HPLC: 100% pure. MS (ESI) $m/z = 336.1$ $[M + 1]^+$. 1H NMR (400 MHz, DMSO- d_6): δ 10.59 (s, 1H), 9.25 (s, 1H), 8.70 (dd, $J = 4.8, 0.8$ Hz, 1H), 8.28 (s, 1H), 8.19 (t, $J = 8.0$ Hz, 1H), 7.97 (d, $J = 8.0$ Hz, 1H),

7.83 (dd, $J = 8.0, 2.0$ Hz, 1H), 7.67 (d, $J = 5.2$ Hz, 1H), 7.38 (d, $J = 8.0$ Hz, 1H), 4.97 (s, 2H), 2.81 (s, 3H).

N-(1-Hydroxy-1,3-dihydrobenzo[*c*][1,2]oxaborol-6-yl)-5-methyl-1-phenyl-1*H*-1,2,3-triazole-4-carboxamide (**24**). The title compound was synthesized according to method B using 5-methyl-1-phenyl-1*H*-1,2,3-triazole-4-carboxylic acid (870.0 mg, 4.3 mmol), 6-aminobenzo[*c*][1,2]oxaborol-1(3*H*)-ol **2** (870.0 mg, 5.8 mmol), HATU (1.7 g, 4.5 mmol), DIPEA (1.7 g, 13.2 mmol), and DMF (16 mL) to yield the crude product, which was purified by preparative HPLC to yield **24** as a white solid (0.61 g, 43%). HPLC: 98% pure. MS (ESI) $m/z = 335$ [M + 1]⁺. ¹H NMR (400 MHz, DMSO-*d*₆): δ 10.56 (s, 1H), 9.27 (s, 1H), 8.29 (s, 1H), 7.84 (dd, $J = 8.0, 2.0$ Hz, 1H), 7.69 (m, 5H), 7.40 (d, $J = 8.4$ Hz, 1H), 4.99 (s, 2H) 2.61 (s, 3H). HRMS (ES⁺): calcd for C₁₇H₁₆B₁N₄O₃ [M+H]⁺ 335.1315, found 335.1319 (1.06 ppm).

N-(1-Hydroxy-1,3-dihydrobenzo[*c*][1,2]oxaborol-6-yl)-1-(6-methoxy-2-pyridin-2-yl)-5-methyl-1*H*-1,2,3-triazole-4-carboxamide (**25**). The title compound was synthesized according to method B using 1-(6-methoxy-2-pyridin-2-yl)-5-methyl-1*H*-1,2,3-triazole-4-carboxylic acid (150.0 mg, 0.6 mmol), 6-aminobenzo[*c*][1,2]oxaborol-1(3*H*)-ol **2** (114.0 mg, 0.77 mmol), HATU (365.0 mg, 1.0 mmol), DIPEA (165.0 mg, 1.3 mmol), and DMF (3 mL) to yield a crude product, which was purified by preparative HPLC to yield **25** as a white solid (134.5 mg, 58%). HPLC: 99% pure. MS (ESI) $m/z = 366.1$ [M+H]⁺. ¹H NMR (400 MHz, DMSO-*d*₆): δ 10.56 (s, 1H), 9.24 (s, 1H), 8.28 (m, 1H), 8.06 (t, $J = 8.0$ Hz, 1H), 7.83 (dd, $J = 8.0, 2.0$ Hz, 1H), 7.58 (d, $J = 7.4$ Hz, 1H), 7.39 (d, $J = 8.4$ Hz, 1H), 7.07 (d, $J = 8.4$ Hz, 1H), 4.98 (s, 2H), 3.95 (s, 3H), 2.91 (s, 3H). HRMS (ES⁺): calcd for C₁₇H₁₇B₁N₅O₄ [M+H]⁺ 366.1374, found 366.1377 (0.93 ppm).

N-(1-Hydroxy-1,3-dihydrobenzo[*c*][1,2]oxaborol-6-yl)-5-methyl-1-(6-methylpyridin-2-yl)-1*H*-1,2,3-triazole-4-carboxamide (**26**). The title compound was synthesized according to method B using 5-methyl-1-(6-methylpyridin-2-yl)-1*H*-1,2,3-triazole-4-carboxylic acid (80.0 mg, 0.4 mmol), 6-aminobenzo[*c*][1,2]oxaborol-1(3*H*)-ol **2** (89.0 mg, 0.6 mmol), HATU (228.0 mg, 0.6 mmol), DIPEA (103.0 mg, 0.8 mmol), and DMF (3 mL) to yield the crude product, which was purified by preparative HPLC to yield **26** as a yellow solid (45 mg, 35%). HPLC: 95% pure. MS (ESI) $m/z = 350.2$ [M+H]⁺. ¹H NMR (400 MHz, DMSO-*d*₆): δ 10.56 (s, 1H), 9.24 (s, 1H), 8.28 (s, 1H), 8.07 (t, $J = 8.0$ Hz, 1H), 7.83 (d, $J = 8.0$ Hz, 1H), 7.75 (d, $J = 8.0$ Hz, 1H), 7.53 (d, $J = 7.6$ Hz, 1H), 7.39 (d, $J = 8.0$ Hz, 1H), 4.98 (s, 2H), 2.82 (s, 3H), 2.59 (s, 3H). HRMS (ES⁺): calcd for C₁₇H₁₇B₁N₅O₃ [M+H]⁺ 350.1424, found 350.1428 (1.01 ppm).

N-(1-Hydroxy-1,3-dihydrobenzo[*c*][1,2]oxaborol-6-yl)-5-methyl-1-(pyridin-3-yl)-1*H*-1,2,3-triazole-4-carboxamide (**27**). The title compound was synthesized according to method B using 5-methyl-1-(pyridin-3-yl)-1*H*-1,2,3-triazole-4-carboxylic acid (150.0 mg, 0.7 mmol), 6-aminobenzo[*c*][1,2]oxaborol-1(3*H*)-ol **2** (109.0 mg, 0.7 mmol), HATU (380 mg, 1.0 mmol), DIPEA (188.0 mg, 1.5 mmol), and DMF (5 mL) to yield the crude product, which was purified by preparative HPLC to yield **27** as a white solid (154.6 mg, 63%). HPLC: 100% pure. MS (ESI) $m/z = 336.2$ [M + 1]⁺. ¹H NMR (400 MHz, DMSO-*d*₆): δ 10.60 (s, 1H), 9.23 (s, 1H), 8.93 (d, $J = 2.4$ Hz, 1H), 8.85 (d, $J = 4.8$ Hz, 1H), 8.28 (d, $J = 1.6$ Hz, 1H), 8.20 (d, $J = 7.6$ Hz, 1H), 7.83 (d, $J = 10.0$ Hz, 1H), 7.74 (m, 1H), 7.39 (d, $J = 8.0$ Hz, 1H), 4.98 (s, 2H), 2.63 (s, 3H). HRMS (ES⁺): calcd for C₁₆H₁₅B₁N₅O₃ [M+H]⁺ 336.1268, found 336.1271 (0.89 ppm).

N-(1-Hydroxy-1,3-dihydrobenzo[*c*][1,2]oxaborol-6-yl)-3-methyl-4-(pyridin-2-yl)furan-2-carboxamide (**28**). To a solution of 3-methyl-4-(pyridin-2-yl)furan-2-carboxylic acid (1.7 g, 8.3 mmol) in DCM (20 mL) was added (COCl)₂ (2.4 mL, 25.1 mmol) and DMF (50 μL). The mixture was stirred at room temperature for 8 h. The mixture was concentrated in a vacuum to give acyl chloride. To a solution of 6-aminobenzo[*c*][1,2]oxaborol-1(3*H*)-ol **2** (1.2 g, 8.1 mmol) and DIPEA (2.9 mL, 16.7 mmol) in THF (30 mL) was added acyl chloride. The mixture was stirred at room temperature for 16 h. Water (150 mL) was added and the mixture was extracted with EtOAc (150 mL × 4). The combined organic extracts were washed with brine (100 mL × 2), dried with anhydrous Na₂SO₄, filtered, and concentrated in a vacuum to give a residue. The residue was purified

by silica gel chromatography (elution with DCM/EtOH = 50: 1) to give a crude product, which was recrystallized from MeCN (100 mL) to yield **28** as a white solid (1.6 g, 57%). HPLC: 98% pure. MS (ESI) $m/z = 335.0$ [M + 1]⁺. ¹H NMR (400 MHz, DMSO-*d*₆): δ 10.20 (s, 1H), 9.24 (s, 1H), 8.65 (d, $J = 4.0$ Hz, 1H), 8.37 (s, 1H), 8.18 (s, 1H), 7.87 (m, 1H), 7.75 (m, 1H), 7.30 (m, 3H), 4.96 (s, 2H), 2.62 (s, 3H).

N-(1-Hydroxy-1,3-dihydrobenzo[*c*][1,2]oxaborol-6-yl)-5-methyl-4-(pyridin-2-yl)furan-2-carboxamide (**29**). To a solution of 5-methyl-4-(pyridin-2-yl)furan-2-carboxylic acid (5.7 g, 28.1 mmol), DIPEA (7.5 g, 58.1 mmol), and HATU (16.0 g, 42.1 mmol) in DMF (60 mL) was added 6-aminobenzo[*c*][1,2]oxaborol-1(3*H*)-ol **2** (4.2 g, 28.2 mmol). The mixture was stirred at room temperature overnight. Water (200 mL) was added and a lot of solid formed. The suspension was filtered and the cake was collected and purified by preparative HPLC to yield **29** as a white solid (6.5 g, 65.6%). HPLC: 100% pure. MS (ESI) $m/z = 334.9$ [M + 1]⁺. ¹H NMR (400 MHz, DMSO-*d*₆): δ 10.20 (s, 1H), 9.27 (s, 1H), 8.65 (d, $J = 4.0$ Hz, 1H), 8.17 (s, 1H), 7.88 (m, 2H), 7.75 (m, 2H), 7.40 (d, $J = 8.4$ Hz, 1H), 7.30 (m, 1H), 4.98 (s, 2H), 2.76 (s, 3H). HRMS (ES⁺): calcd for C₁₈H₁₆B₁N₅O₄ [M+H]⁺ 335.1203, found 335.1206 (0.86 ppm).

N-(1-Hydroxy-1,3-dihydrobenzo[*c*][1,2]oxaborol-6-yl)-3-methyl-4-(pyridin-2-yl)thiophene-2-carboxamide (**30**). The title compound was synthesized according to method B using 3-methyl-4-(pyridin-2-yl)thiophene-2-carboxylic acid (100 mg, 0.46 mmol), 6-aminobenzo[*c*][1,2]oxaborol-1(3*H*)-ol **2** (80 mg, 0.54 mmol), HATU (200 mg, 0.53 mmol), DIPEA (300 mg, 2.33 mmol), and DMF (2 mL) to yield the crude product, which was purified by preparative HPLC to yield **30** as a white solid (63.8 mg). HPLC: 99% pure. MS (ESI) $m/z = 351.1$ [M + 1]⁺. ¹H NMR (400 MHz, DMSO-*d*₆): δ 10.26 (s, 1H), 9.27 (s, 1H), 8.70 (d, $J = 4.0$ Hz, 1H), 8.11 (s, 1H), 8.03 (s, 1H), 7.74 (t, $J = 2.0$ Hz, 1H), 7.70 (m, 2H), 7.40 (m, 2H), 4.98 (s, 2H), 2.55 (s, 3H). HRMS (ES⁺): calcd for C₁₈H₁₆B₁N₂O₃S₁ [M+H]⁺ 351.0975, found 351.0978 (0.94 ppm).

N-(1-Hydroxy-1,3-dihydrobenzo[*c*][1,2]oxaborol-6-yl)-5-(pyridin-2-yl)-1,3,4-oxadiazole-2-carboxamide (**31**). To a reaction mixture of 5-(pyridin-2-yl)-1,3,4-oxadiazole-2-carbonyl chloride were added DIPEA (6.8 g, 52.7 mmol) and a solution of 1-hydroxy-3*H*-2,1-benzoxaborol-6-amine **2** (2.5 g, 17 mmol) in MeCN (50 mL) at 0 °C. The mixture was stirred at 0 °C for 1 h. The reaction mixture was quenched by adding water (100 mL) at room temperature and extracted with EtOAc (100 mL × 2). The combined organic extracts were washed with brine (200 mL × 2), dried over Na₂SO₄, filtered, and concentrated under reduced pressure to give a residue. The residue was dispersed in DCM (20 mL), filtered, and the cake was dried under reduced pressure to give a crude product, which was purified by preparative HPLC to yield **31** as a white solid (1.9 g, 45%). HPLC: 99% pure. MS (ESI) $m/z = 323.2$ [M+H]⁺. ¹H NMR (400 MHz, DMSO-*d*₆): δ 11.36 (s, 1H), 9.32 (s, 1H), 8.84 (d, $J = 2.4$ Hz, 1H), 8.32 (m, 1H), 8.25 (s, 1H), 8.12 (m, 1H), 7.85 (m, 1H), 7.72 (d, $J = 3.6$ Hz, 1H), 7.46 (d, $J = 8.4$ Hz, 1H), 5.00 (s, 2H).

Biology. Compounds and Reagents. For *in vitro* assays, compound stock solutions were prepared in 100% dimethyl sulfoxide (DMSO) at 20 mM. Compounds were serially prediluted (2-fold or 4-fold) in DMSO, followed by a further (intermediate) dilution in demineralized water to assure a final in-test DMSO concentration of <1%. For *in vivo* studies, compounds were formulated in 2% ethanol, 1 mol equiv NaOH, and dextrose (5% solution) when administered orally to mice, hamsters, and dogs or intravenously (pH adjusted to 7) to rats and dogs. For oral administration in rats, 0.5% (w/v) methylcellulose and 0.1% (w/v) sodium dodecyl sulfate in Milli-Q water were used. Miltefosine was formulated in water at 20 mg/mL.

Cell Cultures. Primary peritoneal mouse macrophages (PMM) were collected two days after peritoneal stimulation with a 2% potato starch suspension. MRC5_{SV2} cells (diploid human embryonic lung fibroblasts) were cultured in minimal essential medium (MEM) containing Earle's salts, supplemented with L-glutamine, NaHCO₃, and 5% inactivated fetal calf serum. All cultures and assays were conducted at 37 °C under an atmosphere of 5% CO₂.

Parasites. *L. infantum* (MHOM/MA/67/ITMAP263) and *L. donovani* (MHOM/ET/67/L82) were maintained in the golden (Syrian) hamster (*Mesocricetus auratus*). *Ex vivo* amastigotes were collected from the spleen of an infected donor hamster using two centrifugation purification steps: 230g for 10 min, keeping the supernatant layer, and 4100g for 30 min, keeping the pellet. The spleen parasite burden was assessed using the Stauber technique.²⁵ For *in vitro* assays, the inoculum was prepared in RPMI-1640 medium, supplemented with 200 mM L-glutamine, 16.5 mM NaHCO₃, and 5% inactivated fetal calf serum. For the *in vivo* model, an infection inoculum containing 2×10^7 amastigotes/100 μ L was prepared in phosphate-buffered saline (PBS).

Animals. Female golden hamsters for the *in vivo* model of visceral leishmaniasis were purchased from Janvier, France (body weight 80–100 g). This study using laboratory rodents was carried out in strict accordance with all mandatory guidelines (EU directives, including the Revised Directive 2010/63/EU on the protection of Animals used for Scientific Purposes that came into force on 01/01/2013, and the declaration of Helsinki in its latest version) and was approved by the ethical committee of the University of Antwerp, Belgium (UA-ECD 2011-74). Female golden hamsters for the pharmacokinetic study were purchased from Vital River, Beijing, China. This study was conducted following institutional review and in accordance with institutional and national guidelines at WuXi AppTec (the Institutional Animal Care and Use Committee (IACUC)). Balb/c mice for the *in vivo* model of visceral leishmaniasis (LSHTM) were purchased from Charles River, U.K., and related studies were conducted under license PPL 70/8427 from the U.K. Home Office.

Intramacrophage *L. infantum* and *L. donovani* Assays. The assay was performed in sterile 96-well microtiter plates, each well containing 10 μ L of the compound dilution and 190 μ L of the PMM/amastigote inoculum (3×10^4 cells/ 4.5×10^5 parasites per well). Parasite multiplication was compared to untreated infected controls (100% growth) and uninfected controls (0% growth). After five-day incubation, total parasite burdens were microscopically assessed after staining the cells with a 10% Giemsa solution. The results were expressed as a percentage reduction in parasite burden compared to untreated control wells. EC₅₀ values were determined using an extended dose range (2-fold compound dilutions, 8-point concentration curve). Miltefosine was used as the reference drug.²⁶ For selected compounds, this assay format was also run using the *L. donovani* inoculum.

In Vitro MRC5 and PMM Cytotoxicity Assays. Assays were performed in sterile 96-well microtiter plates, each well containing 10 μ L of the compound dilution and 190 μ L of MRC5_{SV2} or PMM inoculum (3×10^4 cells/mL). Cell growth was compared to untreated controls (100% growth) and assay-media controls (0% growth). After three-day incubation, cell viability was assessed fluorometrically by adding resazurin (50 μ L/well of a stock solution in phosphate buffer (50 μ g/mL)), incubating for 4 h and measuring fluorescence (λ_{ex} 550 nm, λ_{em} 590 nm). The results were expressed as a percentage reduction in cell growth compared to untreated control wells. EC₅₀ values were determined using an extended dose range (2-fold compound dilutions, 8-point concentration curve) to a highest concentration of 64 μ M. Tamoxifen was included as the reference drug.

In Vivo Hamster Model of Visceral Leishmaniasis. Female golden hamsters were randomly allocated to experimental groups of six animals each, based on body weight. At the start of the experiment (Day 0), each animal was infected with *L. infantum* or *L. donovani* inoculum, delivered by intracardial injection. Six hamsters were assigned to the vehicle-treated, infected control group. Six hamsters were assigned per group (1 group/compound) for the evaluation of compound and miltefosine. At Day 21 postinfection (21 dpi), all animals in each group were dosed orally for five (or ten) consecutive days (21–25 dpi): compound was dosed at 25–50 mg/kg b.i.d.; miltefosine was dosed at 40 mg/kg q.d. At Day 35 (10 days after the final oral dose), all animals were euthanized and autopsies were conducted. The study evaluated the following parameters.

1. Adverse effects: all animals were observed daily for the occurrence/presence of adverse effects.
2. Body weight: all animals were weighed twice per week to monitor general health.
3. Parasite burden: amastigote burdens in each target organ (liver, spleen, and bone marrow) were determined at Day 35. The organs of individual animals were weighed (except for bone marrow). Impression smears were stained with Giemsa for microscopic examination of the total amastigote burden, defined as the mean number of amastigotes per cell multiplied by the number of cells counted (minimum 500 nuclei); the results were expressed as a percentage reduction in amastigote burden compared to vehicle-treated, infected control animals.

In Vivo Mouse Model of Visceral Leishmaniasis. Female BALB/c mice were infected with 2×10^7 *L. donovani* amastigotes/0.2 mL i.v. harvested from the spleen of an infected donor RAG1B6 mouse (LSHTM). After 7 days, the mice were treated with miltefosine or DNDI-6148 for 5 consecutive days. Five days after the final dose, mice were humanely killed, liver and spleens were dissected and weighed, and impression smears were made for the calculation of parasite burden (Stauber equation).²⁵

Liver Microsome Stability. Tests were performed by WuXi AppTec, China. Test compounds (at 1 μ M) or positive controls (testosterone, propafenone, and diclofenac) were incubated at 37 °C with liver microsomes from Balb/c mouse, golden (Syrian) hamster, Sprague-Dawley rat, Beagle dog, or human in the presence of a NADPH regenerating system and phosphate buffer (100 mM, pH 7.4) at 0.4 or 0.8 mg/mL microsomal protein. The samples were removed at time intervals from 0 to 60, 90, or 120 min and immediately mixed with cold methanol supplemented or not with acid (3% formic acid) and centrifuged prior to analysis by LC-MS/MS using tolbutamide or propranolol as internal standards.

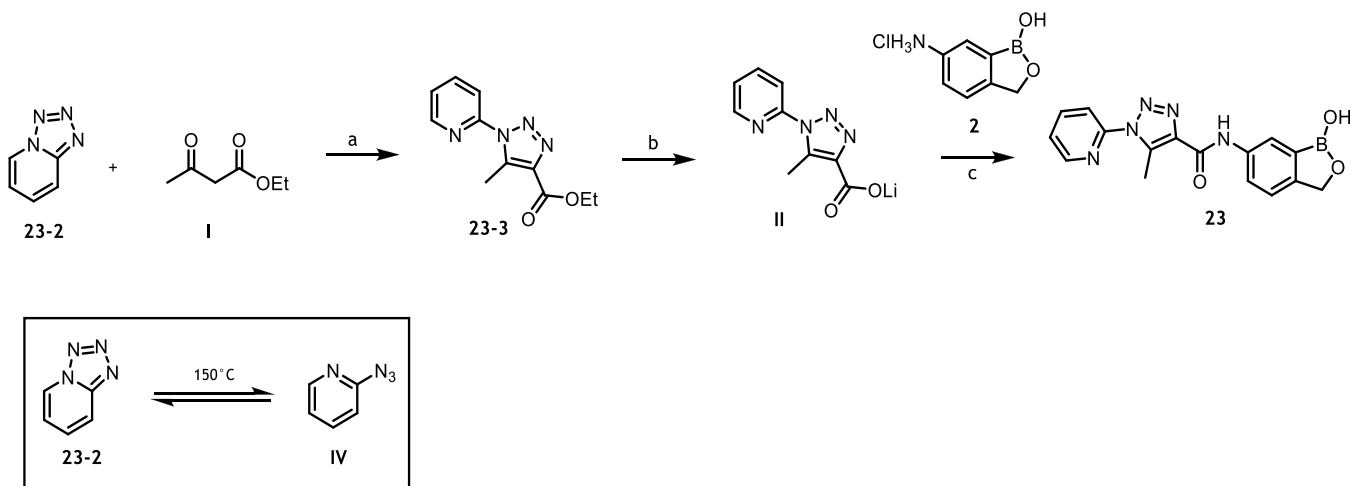
Hepatocyte Stability. Tests were performed by WuXi AppTec, China. Following a viability check of cryopreserved hepatocytes from Sprague-Dawley rat, Beagle dog, or human, test compounds (at 1 μ M) or positive controls 7-ethoxycoumarin and 7-hydroxycoumarin (at 3 μ M) were incubated at 37 °C, 5% CO₂ with hepatocytes in Williams' Medium E. Following incubation of 15, 30, 60, 90, 120, 180, and 240 min, reactions were stopped by the addition of acetonitrile, the samples were centrifuged, and LC-MS/MS analysis was conducted using tolbutamide as an internal standard.

Metabolite ID Studies. Metabolite identification studies were conducted at WuXi AppTec, China. DNDI-6148 was incubated at 10 μ M in the presence of Beagle dog and Sprague-Dawley rat liver microsomes (1 mg/mL) for 60 min. Following precipitation with a solution of formic acid and acetonitrile, metabolites were identified by LC-UV-MSn ($n = 1-2$).

CYP Inhibition Studies. The study was conducted by WuXi AppTec, Co., China, using the time-dependent (TDI) method. For detecting any IC₅₀ shift, the test compound (at concentrations of 0.05–50 μ M) was first preincubated for 30 min at 37 °C with pooled human liver microsomes in the presence or not of NADPH. Following incubation with substrates (phenacetin for 1A2, diclofenac for 2C9, S-(+) mephenytoin for 2C19, dextromethorphan for 2D6, and midazolam or testosterone for 3A4), reactions were stopped by adding ice-cold acetonitrile, the samples were analyzed for the formation of metabolites by LC-MS/MS, and the percentage of inhibition was determined.

hERG Inhibition. An automated patch-clamp method (QPatch HTX) was used by WuXi AppTec, China. Chinese hamster ovary cells expressing hERG potassium channels were incubated at room temperature with test compounds (0.12, 0.37, 1.11, 3.33, 10, and 30 μ M, in triplicate) or amitriptyline as a positive control.

Plasma-Protein Binding. Tests were conducted by WuXi AppTec, Co., China, using the equilibrium dialysis method and a 96-well plate format. The test compound (at 2 μ M, in triplicate) in solution in plasma (Balb/c mouse, golden (Syrian) hamster, Sprague-Dawley rat, Beagle dog or human) was dialyzed against 100 mM phosphate-buffered saline (pH 7.4) on a rotating plate incubated for 6 h at 37

Scheme 5. Synthetic Route to DNDI-6148 (23) Employed for the Material Used in the MoA Studies^a

^aReagents and conditions: (a) NaOEt, EtOH, 150 °C, 2 h (flow), 38%; (b) LiOH, THF/water, room temp., 16 h, 97%; and (c) 2, T3P, DIPEA, DMF/EtOAc, RT, 16 h, 29%.

°C. Following the precipitation of protein with acetonitrile or acetonitrile/methanol containing both 1% phosphoric acid, the amount of compound present in each compartment was quantified by LC-MS/MS.

Thermodynamic Solubility. The thermodynamic solubility was measured by WuXi AppTec, China. Aliquots of the compound DMSO stock (10 mM) were transferred to fasted state simulated intestinal fluid (FaSSIF) buffer (pH 6.5) or fed state simulated intestinal fluid (FeSSIF) buffer (pH 5.0), and the mixtures were shaken for 24 h at room temperature. Following sampling by a Whatman filter device, the compound concentrations were determined by UV spectroscopy.

Membrane Permeability. Bidirectional permeability tests with MDCK-MDR1 cells were performed by WuXi AppTec, Co., China. The test compound, at a concentration of 2 μ M in 0.4% DMSO/HBSS buffer with 10 mM HEPES pH 7.4, was applied to the apical or basolateral side of the cell monolayer. Permeation of the compound from A to B direction or B to A direction was determined in triplicate over a 150 min incubation at 37 °C and 5% CO₂ (95% humidity). Test and reference compounds were quantified by LC-MS/MS analysis based on the peak area ratio of analyte/internal standard.

Ames Assay. Mini-Ames reverse mutation screens were conducted by WuXi AppTec, Co., China. Two *Salmonella typhimurium* strains (TA98 and TA100) were employed, both in the presence and absence of metabolic activation (induced rat liver S9). Test compounds were assessed at doses of 1.5, 4, 10, 25, 64, 160, 400, and 1000 μ g per well, 2-aminoanthracene, 2-nitrofluorene, and sodium azide were used as positive controls, and the negative control was DMSO.

In Vivo Pharmacokinetic Studies. *In vivo* pharmacokinetic studies were conducted at WuXi AppTec, Co., China.

Hamster. Compounds were formulated as a homogenous suspension in 2% ethanol, 1 mol equiv NaOH, dextrose (5% solution), and dosed twice p.o. on a single day (8 h apart, 25 or 50 mg/kg, BID) in female golden Syrian hamsters. The K₂-EDTA anticoagulant was added to blood samples collected from 0.25 to 36 h, which were processed to plasma and stabilized with phosphoric acid (1% final) before analysis by LC-MS/MS. PK parameters were calculated using WinNonlin software (version 6.3).

Rat. DNDI-6148 was formulated in 2% ethanol, 1 mol equiv NaOH, dextrose (5% solution), and administered to male Sprague-Dawley rats, either i.v. after filtration and pH adjustment (at 2 mg/kg), or p.o. as a homogenous suspension (at 10 mg/kg). The K₂-EDTA anticoagulant was added to blood samples collected at predose, 0.083 (i.v. only), 0.25, 0.5, 1, 2 (p.o. only), 4, 8, and 24 h, and were processed to plasma and stabilized with phosphoric acid

(1% final) before analysis by LC-MS/MS. PK parameters were calculated using WinNonlin software (version 6.21 and 6.3).

Dog. DNDI-6148 was administered intravenously at 1 mg/kg and orally at 5 mg/kg to male Beagle dogs. The formulation for the i.v. leg was 2% ethanol, 1.0 mol equiv NaOH, dextrose (5% solution) filtered, and adjusted to pH 7, and for the p.o. leg, the formulation was 2% ethanol, 1.0 mol equiv NaOH, and dextrose (5% solution). The K₂-EDTA anticoagulant was added to blood samples collected at predose, 0.033 (i.v. only), 0.083 (p.o. only), 0.25, 0.5, 1, 3, 6, 9, and 24 h, and were stabilized with phosphoric acid (1% final) before analysis by LC-MS/MS. PK parameters were calculated using WinNonlin software (version 6.3).

MoA Studies. *Synthesis of DNDI-6148, N-(1-Hydroxy-1,3-dihydrobenzo[c][1,2]oxaborol-6-yl)-5-methyl-1-(pyridin-2-yl)-1H-1,2,3-triazole-4-carboxamide (23) Used in MoA studies.* All NMR spectra for the compounds and intermediates made in the course of these studies are available upon request.

The samples of DNDI-6148 used in the MoA studies were prepared using a three-step sequence (Scheme 5) modified from a synthetic route previously reported by Jacobs and co-workers.²⁷ In brief, triazole 23-3 was prepared using an optimized flow chemistry procedure to alleviate the potential risk of explosion when heating low molecular weight organic azides. Note, tetrazole 23-2 is converted to the azide reactant (IV) under the thermal reaction conditions.²⁸ Treatment with LiOH hydrolyzed the ester function of 23-3 to give lithium salt II, which was converted to DNDI-6148 (23) by reaction with aniline 2, T3P, and base.

Ethyl 5-Methyl-1-(pyridin-2-yl)-1H-1,2,3-triazole-4-carboxylate (23-3). A solution of tetrazolo[1,5-a]pyridine (23-2) (144 mg, 1.2 mmol) and ethyl 3-oxobutanoate (I) (1.56 g, 5.99 mmol) in EtOH (10 mL) and a solution of NaOEt (245 mg, 3.6 mmol) in EtOH (10 mL) were mixed in a 1:1 ratio and applied to the flow coil (Vapourtec RS-400 flow chemistry system). The reaction mixture was then heated at 150 °C with a residence time of 2 h. The crude product mixture was collected into a vial and acidified to pH 5 by the addition of HCl (2N aq.). The reaction mixture was then concentrated under reduced pressure and directly purified by silica flash column chromatography (10:90 \rightarrow 50:50 EtOAc:heptane), affording ester 23-3 as a colorless solid (110 mg, 38% yield). ¹H NMR (500 MHz, CDCl₃) δ 8.59 (1H, d, *J* = 4.75 Hz), 8.00–7.93 (2H, m), 7.42 (1H, t, *J* = 6.03 Hz), 4.47 (2H, q, *J* = 7.12 Hz), 2.92 (3H, s), 1.45 (3H, t, *J* = 7.10 Hz). ¹³C NMR (126 MHz, CDCl₃) δ 161.7, 150.2, 148.5, 139.7, 139.1, 137.4, 124.1, 118.3, 61.0, 14.3, 11.0. HRMS (ES⁺): *m/z* [M+H]⁺ calcd for C₁₁H₁₃N₄O₂, 233.1033; found, 233.1061.

Lithium 5-Methyl-1-(pyridin-2-yl)-1H-1,2,3-triazole-4-carboxylate (II). A solution of LiOH (1 M, aq, 0.31 mL, 0.31 mmol) was

added to a solution of ethyl 5-methyl-1-(pyridin-2-yl)-1H-1,2,3-triazole-4-carboxylate (**23-3**) (72 mg, 0.31 mmol) in THF/water (4:1, 10 mL), and the resulting mixture was stirred at room temperature for 16 h. The reaction mixture was then concentrated under reduced pressure, and the resultant aqueous residue was lyophilized to furnish the title compound as a colorless solid (64 mg, 97%). ¹H NMR (500 MHz, D₂O) δ 8.74 (1H, d, *J* = 4.05 Hz), 8.28 (1H, t, *J* = 7.80 Hz), 7.84 (1H, d, *J* = 8.00 Hz), 7.79 (1H, dd, *J* = 7.15, 5.35 Hz), 2.67 (3H, s). ¹³C NMR (126 MHz, D₂O) δ 168.4, 149.0, 147.9, 141.9, 140.7, 137.6, 125.9, 120.6, 9.3. HRMS (ES⁺): *m/z* [M+H]⁺ calcd for C₉H₉N₄O₂, 205.0720; found, 205.0686.

DNDI-6148, *N*-(1-Hydroxy-1,3-dihydrobenzo[*c*][1,2]oxaborol-6-yl)-5-methyl-1-(pyridin-2-yl)-1H-1,2,3-triazole-4-carboxamide (**23**). Neat DIPEA (130 mg, 1.28 mmol) was added to a stirred suspension of carboxylate **II** (45 mg, 0.214 mmol) and 6-aminobenzo[*c*][1,2]-oxaborol-1(3*H*)-ol, hydrochloride (**5**) (59.6 mg, 0.321 mmol) in dry DMF (3.0 mL) at room temperature. A solution of propylphosphonic anhydride (50% w/v in EtOAc, 0.757 mL, 0.642 mmol) was then added dropwise, and the resulting mixture was stirred for a further 16 h at room temperature. The reaction mixture was then concentrated under reduced pressure and directly purified by silica flash column chromatography (2:98 MeOH:CH₂Cl₂), affording the title compound as a colorless solid (21.7 mg, 95% purity, 29% yield). The product was further purified by reverse phase preparative HPLC (C18 silica, 5:95 → 95:5 MeCN:water + 0.1% NH₃) to give an assay/analytical sample at >95% purity. ¹H NMR (400 MHz, DMSO) δ 10.53 (1H, s), 9.20 (1H, s), 8.71 (1H, ddd, *J* = 4.86, 1.78, 0.72 Hz), 8.27 (1H, d, *J* = 1.76 Hz), 8.19 (1H, dt, *J* = 11.79, 1.87 Hz), 7.98 (1H, d, *J* = 8.08 Hz), 7.84 (1H, dd, *J* = 8.22, 2.02 Hz), 7.68 (1H, ddd, *J* = 7.51, 4.87, 0.95 Hz), 7.39 (1H, d, *J* = 8.32 Hz), 4.98 (2H, s), 2.82 (3H, s). ¹³C NMR (126 MHz, DMSO) δ 159.8, 149.8, 149.7, 149.5, 140.5, 139.4, 138.1, 137.7, 125.5, 124.3, 123.0, 121.9, 119.5, 70.2, 10.7 (note, the signal for the benzene quaternary carbon atom directly linked to the boron atom was not observed in the ¹³C NMR due to severe broadening from scalar relaxation caused by the spin dynamics of the quadrupolar ¹¹B nucleus). HRMS (ES⁺): *m/z* [M+H]⁺ calcd for C₁₆H₁₅BN₅O₃, 336.1262; found, 336.1271.

Cell Lines and Culture Conditions. The clonal *L. donovani* cell line LdBOB (derived from MHOM/SD/62/1S-CL2D) was grown as promastigotes at 28 °C, as described previously. Bloodstream form *T. brucei* MiTat 1.2 clone 221a and its derived subline, 2T1, were cultured at 37 °C in the presence of 5% CO₂ in HMI9-T medium, as described previously. *T. brucei* cell lines overexpressing CPSF3 and overexpressing a mutated version of CPSF3 (Asn232His) were generated as part of a previous study and cultured as described.¹⁹

Generation of *L. donovani* Transgenic Cell Lines. *L. donovani* CPSF3 gene (LdBPK_343210.1) was custom synthesized by GeneArt and ligated into the pIR1SAT vector via BglII restriction sites. Using the Q5 mutagenesis kit (NEB) and the pIR1SAT-LdCPSF3^{WT} construct as a template, mutations encoding A655C and Asn219His change to CPSF3^{WT} were introduced. Mutations were introduced using the specific primers 5'-GAGTACACGGCATCCGC-3' and 5'-TCCGCAATCAGGATGCTGGT-3' and as per manufacturers' instructions. Wild-type and mutated pIR1SAT constructs were digested with SwaI and transfected into *L. donovani* promastigotes, as previously described. Resistant clones were selected with nourseothricin (100 μg/mL), and two clones per transfection were selected for further study.

CRISPR-Cas9 Generated Mutations in LdCPSF3. A cell line constitutively expressing Cas9 and T7 RNA polymerase was generated by transfecting 4 × 10⁷ promastigotes with the pTB007 vector (10 μg), as previously described.²⁹ Expression of Cas9 in selected clones was confirmed by western blotting (Figure S1). In addition, the CRISPR-Cas9 system in these parasites was confirmed as functional following the successful tagging of the flagellar protein PF16 with mNeonGreen, as previously described.²⁹

To introduce specific mutations into CPSF3, 3 × 10⁶ promastigotes expressing Cas9 and T7 RNA were resuspended in a 110 μL of Human T-Cell Nucleofector reagent and transfected with 18 μL of sgRNA and 4 μg of template using the Amaxa Nucleofector

electroporator (program V-033). sgRNA was produced according to the previously established protocol from the Gluenz lab,³⁰ in which the scaffold primer G00 and a gene-specific forward primer (FwsgRNA) were used (Table S1). The sgRNA template and templates introducing base edits are summarized in Table S1. Twenty-four hours following transfection, DNDI-6148 was added to cultures at 6 μM. Drug-selected populations were cloned by limiting dilution, EC_{50s} were determined, and genomic DNA was extracted. The CPSF3 gene from CRISPR-edited parasites was amplified by PCR, and the resulting products were sequenced.

In Vitro Drug Sensitivity Assays (MoA Studies). Drug sensitivity assays with wild-type and transgenic *T. brucei* and *L. donovani* cell lines were carried out as previously described.^{31,32}

Confirmation of CPSF3 Overexpression Using MS. WT and *L. donovani* promastigotes (3 × 10⁸) overexpressing CPSF3 were washed twice with PBS (1000 g, 4 °C, 5 min). The pellet was resuspended in 1.5 mL of lysis buffer (50 mM potassium phosphate buffer, pH 7.0, 1 mM EDTA, 1 mM DTT, and 1 × EDTA-free complete protease inhibitors (Roche)). Parasites were biologically inactivated by 3 × freeze/thaw cycles prior to lysis using a One-Shot Cell Disruptor (Constant Systems) at 30 kpsi. Lysed cells were then centrifuged (10 min, 4 °C, 15 000g), and the soluble material was harvested. Soluble cell lysates (100 μg samples) were reduced by the addition of tris(2-carboxyethyl)phosphine hydrochloride (TCEP, 25 mM final concentration) and incubated at 37 °C for 10 min. The samples were then alkylated by the addition of iodoacetamide (25 mM final concentration) and incubated at RT for 1 h in the dark. Alkylated samples were digested by the addition of 1:50 endoproteinase LysC (Wako, Japan) in 100 mM triethylammonium bicarbonate (TEAB), followed by incubation at 37 °C for 6 h, then the addition of 1:50 trypsin (1.50 dilution) and incubation at 37 °C overnight. The resulting digested peptides were then vacuum-dried.

LC-MS/MS Analysis. Analysis of peptides was performed on a Q-Exactive Plus mass spectrometer (Thermo Scientific) coupled with a Dionex Ultimate 3000 RS (Thermo Scientific). LC buffers used were as follows: Buffer A (0.1% formic acid in Milli-Q water (v/v)) and Buffer B (80% acetonitrile and 0.1% formic acid in Milli-Q water (v/v)). Aliquots (15 μL per sample) were loaded at 10 μL/min onto a PepMap nanoViper C18 column (100 μm × 2 cm, 5 μm, 100 Å, Thermo Scientific) equilibrated with 98% Buffer A. The column was washed for 5 min at the same flow rate and then switched in line with a Thermo Scientific, resolving PepMap RSLC C18 column (75 μm × 50 cm, 2 μm, 100 Å). Peptides were eluted at a constant flow rate of 300 nL/min with a linear gradient of 2–35% Buffer B in 125 min, then to 98% in 127 min. The column was then washed with 98% Buffer B for 20 min and re-equilibrated in 2% Buffer B for 17 min prior to loading the next sample. The Q-Exactive Plus was used in the data-dependent mode. The scan cycle comprised MS1 scan (*m/z* range from 335–1600, with a maximum ion injection time of 20 ms, a resolution of 70 000, and an automatic gain control (AGC) value of 1 × 10⁶), followed by 15 sequential dependent MS2 scans (with an isolation window set to 1.4 Da, resolution at 17 500, maximum ion injection time at 100 ms, and AGC 2 × 10⁵). The stepped collision energy was set to 27 and fixed first mass to 100 *m/z*. Spectra were acquired in a centroid mode and unassigned charge states. Charge states above 6, as well as singly charged species, were rejected. To ensure mass accuracy, the mass spectrometer was calibrated on day 1 of the analyses. LC-MS analysis was performed by the FingerPrints Proteomics Facility (University of Dundee).

Data Analysis. MS data analysis was performed using MaxQuant software (<http://maxquant.org/>, version 1.6.2.6a). Carbamidomethyl (C), oxidation (M), acetyl (Protein N-term), deamidation (NQ), and Gln → pyro-Glu were set as variable modifications. Proteins were identified by searching a protein sequence database containing *T. brucei brucei* TREU927 annotated proteins (downloaded from TriTrypDB 46, <http://www.tritrypdb.org>). LFQ and “match between runs” features were enabled. Trypsin/P and LysC/P were selected as the specific proteases with two potential missed cleavages. The FDR threshold for peptides and proteins was 0.01. FTMS MS/MS mass tolerance was set to 10 ppm, and ITMS MS/MS mass tolerance was

0.6 Da. Protein abundance was obtained using LFQ intensity values. LFQ intensities were calculated using at least 2 unique peptides. Data was visualized using Perseus 1.6.2.1 (<https://maxquant.org/perseus/>).

Homology Modeling and *In Silico* Docking Studies. To identify suitable template structures for the generation of the *L. donovani* CPSF3 homology model, the sequence UniProtKB—E9BRB9 was used to query the PDB using “BLAST” as implemented in the NCBI blastp suite (<https://blast.ncbi.nlm.nih.gov/>). Endonucleases from five different species, human CPSF73 (PDB code 2I7T and 6M8Q—sequence identity 54%), *Saccharomyces cerevisiae* CPSF (PDB code 6I1D—sequence identity 47%), *Pyrococcus horikoshii* CPSF3 (PDB code 3AF5—sequence identity 29%), *Cryptosporidium hominis* (PDB code 6Q55—sequence identity 48%), and *T. thermophilus* TTHA0252 (several structures available exemplified by PDB code 3IEM—sequence identity 30%), were identified as close analogues that could be used as template structures. The *T. thermophilus* structure is complexed with a stable RNA analogue bound to the catalytic site located at the interface between the metallo- β -lactamase and β -CASP domains, whereas one human, *S. cerevisiae* and *P. horikoshii* structures are apo forms where the Zn²⁺-containing binding site is inaccessible. The *C. hominis* structure is in complex with a small boron-containing inhibitor (AN3661) and where the binding site is still inaccessible to a larger ligand. One of the human structures (6M8Q) is in complex with a small ligand that does not interact with the two Zn²⁺ ions and adopts the binding mode that causes structural rearrangements in loop regions adjacent to the binding cavity. Thus, the *T. thermophilus* structure was selected as a suitable template. The alignment between the amino acid sequence of *LdCPSF3* that of the *T. thermophilus* CPSF3 was manually curated (Figure S5) and showed a sequence identity of 68% in the binding site area. A homology model for *LdCPSF3* was built using the knowledge-based method in Prime in Schrödinger (Schrödinger Release 2019-3: Schrödinger, LLC, New York, NY, 2020). Zinc atoms were modeled into the structure but not the RNA substrate. Due to its empty p-orbital, the boron atom in DNDI-6148 is a strong electrophile (Lewis acid) that can react with solvent water molecules. The nucleophilic attack of an activated water molecule on the trigonal boron atom leads to the formation of a tetrahedral negatively charged boron species. The three-dimensional structure of the hydroxylated form of DNDI-6148 was built in Maestro, minimized with the OPLS3 force field, and docked in the catalytic site of the *LdCPSF3* model using GLIDE in Schrödinger. Docking results were subjected to a restrained minimization procedure with the OPLS3e force field, as implemented, where each heavy atom was allowed to deviate by up to 0.5 Å from its original position in the model.

■ ASSOCIATED CONTENT

Supporting Information

The Supporting Information is available free of charge at <https://pubs.acs.org/doi/10.1021/acs.jmedchem.1c01437>.

Chemistry experimental details for all compounds, Supplementary figures and tables related to MoA and docking studies; HPLC chromatograms of key compounds used *in vivo*; and data illustrating the PK properties of compound 23 in rat and dog and off-target profiling of compound 23 (PDF)

String data for all compounds (CSV)

DNDI-6148 rat and dog PK data (XLSX)

Compound 23 docked into *LdCPSF3* (PDB)

■ AUTHOR INFORMATION

Corresponding Authors

Charles E. Mowbray – *Drugs for Neglected Diseases initiative (DNDi), 1202 Geneva, Switzerland*; orcid.org/0000-0003-3538-8116; Email: cmowbury@dndi.org

Susan Wyllie – *Division of Biological Chemistry and Drug Discovery, Wellcome Centre for Anti-infectives Research, School of Life Sciences, University of Dundee, Dundee DD1 5EH, U.K.*; orcid.org/0000-0001-8810-5605; Email: s.wyllie@dundee.ac.uk

Authors

Stéphanie Brillard – *Drugs for Neglected Diseases initiative (DNDi), 1202 Geneva, Switzerland*

Paul A. Glossop – *Sandexis Medicinal Chemistry Ltd, Kent CT13 9ND, U.K.*; orcid.org/0000-0001-6567-5648

Gavin A. Whitlock – *Sandexis Medicinal Chemistry Ltd, Kent CT13 9ND, U.K.*

Robert T. Jacobs – *Scynexis, Durham, North Carolina 27713, United States*; orcid.org/0000-0001-9669-2862

Jason Speake – *Scynexis, Durham, North Carolina 27713, United States*

Bharathi Pandi – *Scynexis, Durham, North Carolina 27713, United States*

Bakela Nare – *Scynexis, Durham, North Carolina 27713, United States*

Louis Maes – *Laboratory for Microbiology, Parasitology and Hygiene (LMPH), University of Antwerp, 2610 Wilrijk, Antwerp, Belgium*

Vanessa Yardley – *Faculty of Infectious and Tropical Diseases, London School of Hygiene & Tropical Medicine, London WC1E 7HT, U.K.*

Yvonne Freund – *Anacor Pharmaceuticals, Palo Alto, California 94303, United States*

Richard J. Wall – *Division of Biological Chemistry and Drug Discovery, Wellcome Centre for Anti-infectives Research, School of Life Sciences, University of Dundee, Dundee DD1 5EH, U.K.*

Sandra Carvalho – *Division of Biological Chemistry and Drug Discovery, Wellcome Centre for Anti-infectives Research, School of Life Sciences, University of Dundee, Dundee DD1 5EH, U.K.*

Davide Bello – *Division of Biological Chemistry and Drug Discovery, Wellcome Centre for Anti-infectives Research, School of Life Sciences, University of Dundee, Dundee DD1 5EH, U.K.*

Magali Van den Kerkhof – *Laboratory for Microbiology, Parasitology and Hygiene (LMPH), University of Antwerp, 2610 Wilrijk, Antwerp, Belgium*

Guy Caljon – *Laboratory for Microbiology, Parasitology and Hygiene (LMPH), University of Antwerp, 2610 Wilrijk, Antwerp, Belgium*

Ian H. Gilbert – *Division of Biological Chemistry and Drug Discovery, Wellcome Centre for Anti-infectives Research, School of Life Sciences, University of Dundee, Dundee DD1 5EH, U.K.*; orcid.org/0000-0002-5238-1314

Victoriano Corpas-Lopez – *Division of Biological Chemistry and Drug Discovery, Wellcome Centre for Anti-infectives Research, School of Life Sciences, University of Dundee, Dundee DD1 5EH, U.K.*

Iva Lukac – *Division of Biological Chemistry and Drug Discovery, Wellcome Centre for Anti-infectives Research, School of Life Sciences, University of Dundee, Dundee DD1 5EH, U.K.*

Stephen Patterson – *Division of Biological Chemistry and Drug Discovery, Wellcome Centre for Anti-infectives Research, School of Life Sciences, University of Dundee, Dundee DD1 5EH, U.K.*

Fabio Zuccotto – Division of Biological Chemistry and Drug Discovery, Wellcome Centre for Anti-infectives Research, School of Life Sciences, University of Dundee, Dundee DD1 5EH, U.K.; orcid.org/0000-0002-3888-7423

Complete contact information is available at:
<https://pubs.acs.org/10.1021/acs.jmedchem.1c01437>

Author Contributions

P.A.G., G.A.W., and S.W. prepared this manuscript on behalf of all the authors. All authors have given approval to the final version of the manuscript.

Funding

The authors gratefully acknowledge financial support for this work from U.K. aid, U.K.; the Bill & Melinda Gates Foundation; and the Federal Ministry of Education and Research (BMBF) through KfW, Germany. For its overall mission, DNDi also receives financial support from Médecins sans Frontières (MSF) International; and the Swiss Agency for Development and Cooperation (SDC), Switzerland. Work carried out at the University of Dundee was funded by the following Wellcome Trust grants: 105021, 203134/Z/16/Z, 218448/Z/19/Z.

Notes

The authors declare no competing financial interest.

ACKNOWLEDGMENTS

The DNDi thanks the staff of SCYNEXIS Inc., WuXi AppTech, LMPH, LSHTM, and the University of Dundee for their individual practical contributions to this work. The Mode of Action group, University of Dundee, would like to thank Professor David Horn and Dr. Eva Rico Vidal for allowing us to use their CRISPR-Cas9 edited *T. brucei* cell line. In addition, they would like to thank the FingerPrints Proteomics Facility at the University of Dundee for assistance with proteomic studies.

ABBREVIATIONS USED

CC₅₀, half-maximum cytotoxic concentration; Cl_{int}, intrinsic clearance; CPSF3, cleavage and polyadenylation specificity factor subunit 3; DNDi, Drugs for Neglected Diseases initiative; FaSSIF, fasted state simulated intestinal fluid; FeSSIF, fed state simulated intestinal fluid; HLM, human liver microsomes; HamLM, hamster liver microsomes; LAB, liposomal amphotericin B; MoA, mode of action; MRC5, human fetal lung fibroblasts; PM, paromomycin; PMM, primary mouse macrophages; SI, selectivity index; SSG, sodium stibogluconate; TCP, target candidate profile; TPP, target product profile; VL, visceral leishmaniasis

REFERENCES

- (1) Alvar, J.; Yactayo, S.; Bern, C. Leishmaniasis and poverty. *Trends Parasitol.* **2006**, *22*, 552–557.
- (2) Alvar, J.; Vélez, I. D.; Bern, C.; Herrero, M.; Desjeux, P.; Cano, J.; Jannin, J.; den Boer, M. Leishmaniasis worldwide and global estimates of its incidence. *PLoS One* **2012**, *7*, No. e35671.
- (3) WHO Leishmaniasis fact sheet. <https://www.who.int/news-room/fact-sheets/detail/leishmaniasis>.
- (4) Berman, J. Visceral leishmaniasis in the New World & Africa. *Indian J. Med. Res.* **2006**, *123*, 289–294.
- (5) DNDi Current treatments for leishmaniasis. <https://dndi.org/diseases/visceral-leishmaniasis/facts/>.
- (6) Alves, F.; Bilbe, G.; Blesson, S.; Goyal, V.; Monnerat, S.; Mowbray, C.; Muthoni Ouattara, G.; Pécou, B.; Rijal, S.; Rode, J;

Solomos, A.; Strub-Wourgaft, N.; Wasunna, M.; Wells, S.; Zijlstra, E. E.; Arana, B.; Alvar, J. Recent Development of visceral leishmaniasis treatments: successes, pitfalls, and perspectives. *Clin. Microbiol. Rev.* **2018**, *31*, No. e00048-18.

(7) Wyllie, S.; Roberts, A. J.; Norval, S.; Patterson, S.; Foth, B. J.; Berriman, M.; Read, K. D.; Fairlamb, A. H. Activation of bicyclic nitro-drugs by a novel nitroreductase (NTR2) in *Leishmania*. *PLoS Pathog.* **2016**, *12*, No. e1005971.

(8) Wyllie, S.; Thomas, M.; Patterson, S.; Crouch, S.; De Rycker, M.; Lowe, R.; Gresham, S.; Urbaniak, M. D.; Otto, T. D.; Stojanovski, L.; Simeons, F. R. C.; Manthri, S.; MacLean, L. M.; Zuccotto, F.; Homeyer, N.; Pflaumer, H.; Boesche, M.; Sastry, L.; Connolly, P.; Albrecht, S.; Berriman, M.; Drewes, G.; Gray, D. W.; Ghidelli-Disse, S.; Dixon, S.; Fiandor, J. M.; Wyatt, P. G.; Ferguson, M. A. J.; Fairlamb, A. H.; Miles, T. J.; Read, K. D.; Gilbert, I. H. Cyclin-dependent kinase 12 is a drug target for visceral leishmaniasis. *Nature* **2018**, *560*, 192–197.

(9) Wyllie, S.; Brand, S.; Thomas, M.; De Rycker, M.; Chung, C. W.; Pena, I.; Bingham, R. P.; Bueren-Calabuig, J. A.; Cantizani, J.; Cebrían, D.; Craggs, P. D.; Ferguson, L.; Goswami, P.; Hobrath, J.; Howe, J.; Jeacock, L.; Ko, E. J.; Korczynska, J.; MacLean, L.; Manthri, S.; Martinez, M. S.; Mata-Cantero, L.; Moniz, S.; Nühs, A.; Osuna-Cabello, M.; Pinto, E.; Riley, J.; Robinson, S.; Rowland, P.; Simeons, F. R. C.; Shishikura, Y.; Spinks, D.; Stojanovski, L.; Thomas, J.; Thompson, S.; Viayna Gaza, E.; Wall, R. J.; Zuccotto, F.; Horn, D.; Ferguson, M. A. J.; Fairlamb, A. H.; Fiandor, J. M.; Martin, J.; Gray, D. W.; Miles, T. J.; Gilbert, I. H.; Read, K. D.; Marco, M.; Wyatt, P. G. Preclinical candidate for the treatment of visceral leishmaniasis that acts through proteasome inhibition. *Proc. Natl. Acad. Sci. U.S.A.* **2019**, *116*, 9318–9323.

(10) Nagle, A. J.; Biggart, A.; Be, C.; Srinivas, H.; Hein, A.; Caridha, D.; Sciotti, R. J.; Pybus, B.; Kreishman-Deitrick, M.; Bursulaya, B.; Lai, Y. H.; Gao, M. Y.; Liang, F.; Mathison, C. J. N.; Liu, X.; Yeh, V.; Smith, J.; Lerario, I.; Xie, Y.; Chianelli, D.; Gibney, M.; Berman, A.; Chen, Y. L.; Jiricek, J.; Davis, L. C.; Liu, X.; Ballard, J.; Khare, S.; Eggimann, F. K.; Luneau, A.; Groessl, T.; Shapiro, M.; Richmond, W.; Johnson, K.; Rudewicz, P. J.; Rao, S. P. S.; Thompson, C.; Tuntland, T.; Spraggon, G.; Glynne, R. J.; Supek, F.; Wiesmann, C.; Molteni, V. Discovery and characterization of clinical candidate LXE408 as a kinetoplastid-selective proteasome inhibitor for the treatment of leishmaniasis. *J. Med. Chem.* **2020**, *63*, 10773–10781.

(11) DNDi Acoziborole factsheet. <https://dndi.org/research-development/portfolio/acoziborole/>.

(12) Jacobs, R. T.; Nare, B.; Wring, S. A.; Orr, M. D.; Chen, D.; Sligar, J. M.; Jenks, M. X.; Noe, R. A.; Bowling, T. S.; Mercer, L. T.; Rewerts, C.; Gaukel, E.; Owens, J.; Parham, R.; Randolph, R.; Beaudet, B.; Bacchi, C. J.; Yarlett, N.; Plattner, J. J.; Freund, Y.; Ding, C.; Akama, T.; Zhang, Y. K.; Brun, R.; Kaiser, M.; Scandale, I.; Don, R. SCYX-7158, an orally-active benzoxaborole for the treatment of stage 2 human African trypanosomiasis. *PLoS Neglected Trop. Dis.* **2011**, *5*, No. e1151.

(13) Nare, B.; Wring, S.; Bacchi, C.; Beaudet, B.; Bowling, T.; Brun, R.; Chen, D.; Ding, C.; Freund, Y.; Gaukel, E.; Hussain, A.; Jarnagin, K.; Jenks, M.; Kaiser, M.; Mercer, L.; Mejia, E.; Noe, A.; Orr, M.; Parham, R.; Plattner, J.; Randolph, R.; Rattendi, D.; Rewerts, C.; Sligar, J.; Yarlett, N.; Don, R.; Jacobs, R. Discovery of novel orally bioavailable oxaborole 6-carboxamides that demonstrate cure in a murine model of late-stage central nervous system african trypanosomiasis. *Antimicrob. Agents Chemother.* **2010**, *54*, 4379–4388.

(14) Van den Kerkhof, M.; Mabile, D.; Chatelain, E.; Mowbray, C. E.; Braillard, S.; Hendrickx, S.; Maes, L.; Caljon, G. In vitro and in vivo pharmacodynamics of three novel antileishmanial lead series. *Int. J. Parasitol.: Drugs Drug Resist.* **2018**, *8*, 81–86.

(15) Hann, M. M. Molecular obesity, potency and other addictions in drug discovery. In *Multifaceted Roles of Crystallography in Modern Drug Discovery*; Scapin, G.; Patel, D.; Arnold, E., Eds.; Springer: Dordrecht, 2015; pp 183–196.

(16) Peterson, L. A. Reactive metabolites in the biotransformation of molecules containing a furan ring. *Chem. Res. Toxicol.* **2013**, *26*, 6–25.

- (17) Wall, R. J.; Moniz, S.; Thomas, M. G.; Norval, S.; Ko, E. J.; Marco, M.; Miles, T. J.; Gilbert, I. H.; Horn, D.; Fairlamb, A. H.; Wyllie, S. Antitrypanosomal 8-hydroxy-naphthyridines are chelators of divalent transition metals. *Antimicrob. Agents Chemother.* **2018**, *62*, No. e00235-18.
- (18) Begolo, D.; Vincent, I. M.; Giordani, F.; Pöhner, I.; Witty, M. J.; Rowan, T. G.; Bengaly, Z.; Gillingwater, K.; Freund, Y.; Wade, R. C.; Barrett, M. P.; Clayton, C. The trypanocidal benzoxaborole AN7973 inhibits trypanosome mRNA processing. *PLoS Pathog.* **2018**, *14*, No. e1007315.
- (19) Wall, R. J.; Rico, E.; Lukac, I.; Zuccotto, F.; Elg, S.; Gilbert, I. H.; Freund, Y.; Alley, M. R. K.; Field, M. C.; Wyllie, S.; Horn, D. Clinical and veterinary trypanocidal benzoxaboroles target CPSF3. *Proc. Natl. Acad. Sci. U.S.A.* **2018**, *115*, 9616–9621.
- (20) Sonoiki, E.; Ng, C. L.; Lee, M. C.; Guo, D.; Zhang, Y. K.; Zhou, Y.; Alley, M. R.; Ahyong, V.; Sanz, L. M.; Lafuente-Monasterio, M. J.; Dong, C.; Schupp, P. G.; Gut, J.; Legac, J.; Cooper, R. A.; Gamo, F. J.; DeRisi, J.; Freund, Y. R.; Fidock, D. A.; Rosenthal, P. J. A potent antimalarial benzoxaborole targets a Plasmodium falciparum cleavage and polyadenylation specificity factor homologue. *Nat. Commun.* **2017**, *8*, No. 14574.
- (21) Bellini, V.; Swale, C.; Brenier-Pinchart, M. P.; Pezier, T.; Georgeault, S.; Laurent, F.; Hakimi, M. A.; Bougdour, A. Target identification of an antimalarial oxaborole identifies AN13762 as an alternative chemotype for targeting CPSF3 in apicomplexan parasites. *iScience* **2020**, *23*, No. 101871.
- (22) Corpas-Lopez, V.; Moniz, S.; Thomas, M.; Wall, R. J.; Torrie, L. S.; Zander-Dinse, D.; Tinti, M.; Brand, S.; Stojanovski, L.; Manthri, S.; Hallyburton, I.; Zuccotto, F.; Wyatt, P. G.; De Rycker, M.; Horn, D.; Ferguson, M. A. J.; Clos, J.; Read, K. D.; Fairlamb, A. H.; Gilbert, I. H.; Wyllie, S. Pharmacological validation of N-myristoyltransferase as a drug target in *Leishmania donovani*. *ACS Infect. Dis.* **2019**, *5*, 111–122.
- (23) Van den Kerkhof, M.; Leprohon, P.; Mabile, D.; Hendrickx, S.; Tulloch, L. B.; Wall, R. J.; Wyllie, S.; Chatelain, E.; Mowbray, C. E.; Braillard, S.; Ouellette, M.; Maes, L.; Caljon, G. Identification of resistance determinants for a promising antileishmanial oxaborole series. *Microorganisms* **2021**, *9*, 1408.
- (24) Van Boclaer, K.; Caridha, D.; Black, C.; Vesely, B.; Leed, S.; Sciotti, R. J.; Wijnant, G. J.; Yardley, V.; Braillard, S.; Mowbray, C. E.; Ioset, J. R.; Croft, S. L. Novel benzoxaborole, nitroimidazole and aminopyrazoles with activity against experimental cutaneous leishmaniasis. *Int. J. Parasitol.: Drugs Drug Resist.* **2019**, *11*, 129–138.
- (25) Stauber, L. A. *Host Resistance to the Khartoum Strain of Leishmania donovani*; The Rice University Pamphlet, 1958; Vol. 45, pp 80–96.
- (26) Jha, T. K.; Sundar, S.; Thakur, C. P.; Bachmann, P.; Karbwang, J.; Fischer, C.; Voss, A.; Berman, J. Miltefosine, an oral agent, for the treatment of Indian visceral leishmaniasis. *N. Engl. J. Med.* **1999**, *341*, 1795–1800.
- (27) Jacobs, R. T. L. Y.; Sciotti, R. J.; Robinson, S. J.; Mowbray, C. E.; Whitlock, G. A.; Speake, J. D.; Glossop, P. A.; Launay, D. F. M. WO2018160845 - Novel oxaborole analogues and uses thereof. 2018.
- (28) Wentrup, C. W.; Winter, H. W. Isolation of diazacycloheptate-trienes from thermal nitrene-nitrene rearrangements. *J. Am. Chem. Soc.* **1980**, *102*, 6159–6161.
- (29) Beneke, T.; Madden, R.; Makin, L.; Valli, J.; Sunter, J.; Gluenz, E. A CRISPR Cas9 high-throughput genome editing toolkit for kinetoplastids. *R. Soc. Open Sci.* **2017**, *4*, No. 170095.
- (30) Beneke, T.; Gluenz, E. LeishGEdit: A method for rapid gene knockout and tagging using CRISPR-Cas9. In *Methods in Molecular Biology*; Humana Press: New York, NY, 2019; Vol. 1971, pp 189–210.
- (31) Jones, D. C.; Hallyburton, I.; Stojanovski, L.; Read, K. D.; Frearson, J. A.; Fairlamb, A. H. Identification of a κ -opioid agonist as a potent and selective lead for drug development against human African trypanosomiasis. *Biochem. Pharmacol.* **2010**, *80*, 1478–1486.
- (32) Wyllie, S.; Patterson, S.; Stojanovski, L.; Simeons, F. R.; Norval, S.; Kime, R.; Read, K. D.; Fairlamb, A. H. The anti-trypanosome drug

fexinidazole shows potential for treating visceral leishmaniasis. *Sci. Transl. Med.* **2012**, *4*, No. 119re1.